CHALMERS
UNIVERSITY OF TECHNOLOGY

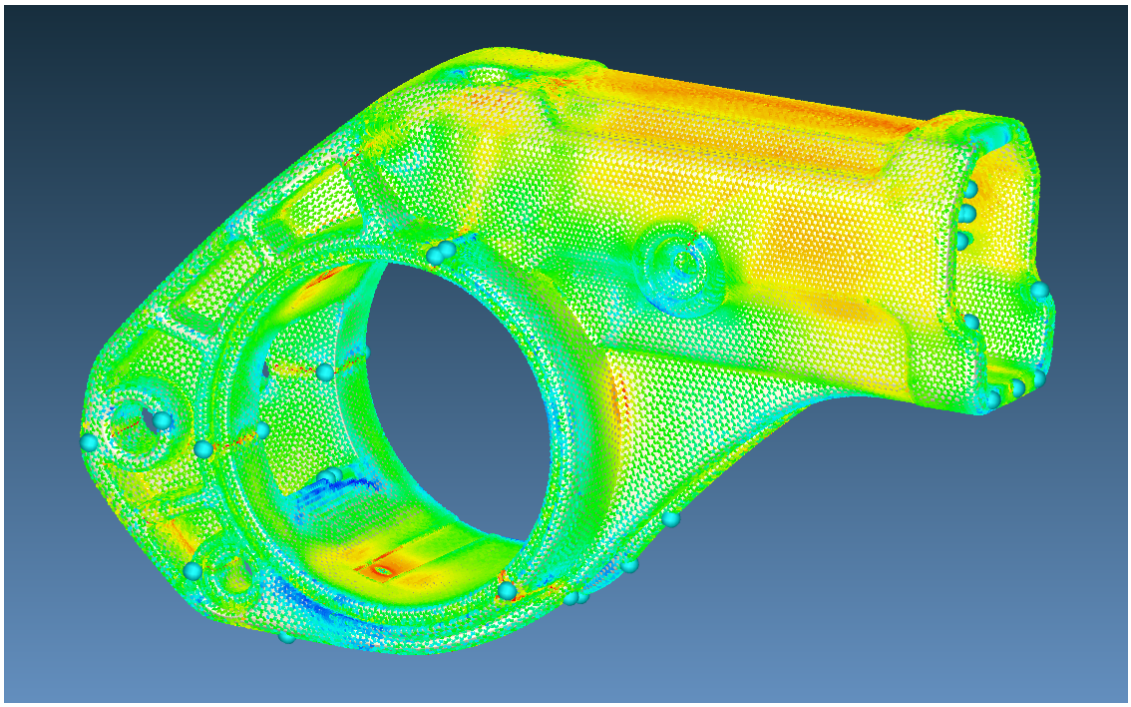

Considering Anisotropic Behaviour and Process Induced Weaknesses in Fibre Reinforced Polymers in CAE

A comparison of material models for fibre reinforced materials in LS-DYNA

Master's thesis in Materials Engineering

GUSTAV HINDÉR

DEPARTMENT OF INDUSTRIAL AND MATERIALS SCIENCE

CHALMERS UNIVERSITY OF TECHNOLOGY
Gothenburg, Sweden 2021
www.chalmers.se

Master's thesis 2021

Considering Anisotropic Behaviour and Process Induced Weaknesses in Fibre Reinforced Polymers in CAE

A comparison of material models for fibre reinforced materials in LS-DYNA

GUSTAV HINDÉR

CHALMERS
UNIVERSITY OF TECHNOLOGY

Department of Industrial and Materials Science
Chalmers University of Technology
Gothenburg, Sweden 2021

Considering Anisotropic Behaviour and Process Induced Weaknesses in Fibre Reinforced Polymers in CAE
A comparison of material models for fibre reinforced materials in LS-DYNA
GUSATV HINDÉR

Supervisor: Henrik Alm, Thule
Supervisor: Antal Boldizar, Department of Industrial and Materials Science
Examiner: Antal Boldizar, Department of Industrial and Materials Science

Master's Thesis 2021
Department of Industrial and Materials Science
Chalmers University of Technology
SE-412 96 Gothenburg
Telephone +46 31 772 1000

Cover:

Typeset in LaTeX
Printed by Chalmers Reproservice
Gothenburg, Sweden 2021

Considering Anisotropic Behaviour and Process Induced Weaknesses in Fibre Reinforced Polymers in CAE
A Comparison of material models for fibre reinforced materials in LS-DYNA
GUSTAV HINDÉR
Department of Industrial and Materials Science
Chalmers University of Technology

Abstract

Computer Aided Engineering (CAE) is widely used for developing new products nowadays. Through advanced software, it is possible to simulate the reality in the computer to save time and money when less component testing is needed. Two examples of CAE are Finite Element Analysis (FEA) and Mould Fill Simulation (MFS). MFS can be used to simulates the melt flow in the mould of an injection moulding process and FEA can be used to structurally analyse components when subjected to various loads. This thesis work was conducted at Thule to investigate the possibility of consider the anisotropic behaviour and process induced weaknesses of short fiber reinforced polymers (SFRP) through MFS in Moldex3D with a subsequent FEA in LS-DYNA. The MFS results was implemented in the FEA through the usage of material models Mat_157 and Mat_215 which are designed for fibre reinforced materials. A tensile test using Polyamide 6 reinforced with 30 wt% short glass fibres (PA6 GF30) specimens was performed and compared with results from the corresponding MFS and FEA. A subsequent Case Study on Thule's Outway Hanging Bike Rack was performed, which also included physical testing, MFS and FEA. Results indicate that it is possible to capture the anisotropic behaviour of SFRP by obtaining the fibre orientation through MFS. Also, some process induced weaknesses, especially weld lines and air traps can be obtained from MFS. In the FEA, the comparison of material models shows that the implementation of fibre orientation can increase the reliability of the analysis, but there is a need for material testing with combined calibration of the material models before they can be implemented in the daily calculations at Thule.

Keywords: Polyamide 6, short glass fiber reinforced polymers, anisotropy, weld lines, air traps, structural analysis, FEM, material models, mould fill simulation.

Acknowledgements

I would like to take this opportunity to thank Thule for giving me the opportunity to conduct an interesting master's thesis with the structural analysis division at the company. It has given me a broader spectrum of the development process and a closer understanding of the relation between materials and CAE. A special thanks to my supervisor at Thule, Henrik Alm, who has contributed the work with extensive knowledge and performed the conducted simulations which has made this work possible. Henrik has also been a great source for guidance and discussion of all the results we obtained during the project. I would also like to thank my supervisor at Chalmers University of Technology, Antal Boldizar for the valuable input regrading the academic aspects of the work.

Gustav Hindér, Gothenburg, June 2021

Contents

List of Figures

List of Tables

1

Introduction

Computer Aided Engineering (CAE) is a tool widely used in the industry to improve productivity and lower the cost of development of new products. By using advanced computational software for Finite Element Analysis (FEA), it is possible to foresee the strengths and weaknesses of products before physical testing of them. However, as the development of materials moves on and they become more advanced it gets more difficult to capture the characteristics of them. If a correct material model is used in the FEM analysis, the risk of discovering costly problems in the end of the development process will be minimized. This Master's thesis will investigate how the anisotropic behaviour and process-induced weaknesses can be predicted and included in the material models for CAE.

1.1 The Company - Thule

Thule was founded in 1942 in Hillerstorp, Småland, where the development and test center is located today. Thule has around 2300 employees around the world. The main focus of Thule is to provide products making it easy for the customers to bring whatever equipment is needed on an adventurous trip. Included in the range of products are bike racks, roof cargo carriers, strollers, backpacks and much more.

1.2 Problem Description

At the global development centre of Thule Group in Hillerstorp Sweden, all the major product categories of the Thule brand are developed and tested. Due to high demands on the structural integrity of the products, simulations are a vital tool that is used throughout the development process. The accuracy of the FEA is highly dependent on the accuracy of the material models used in the simulations. For critical components, it is vital to be able to consider the anisotropic behaviour and process-induced weaknesses early in the product development process.

Current material models used in the simulations of injection molded components in short glass fiber reinforced polymers at Thule consider the material to be homogeneous and isotropic without any defects. Nevertheless, defects induced during the injection molding process are not uncommon and should be considered along with

the anisotropic behaviour caused by the reinforcement to obtain a more accurate result in the FEA.

1.3 Purpose and Goals

The purpose of this master's thesis is to investigate how the anisotropic behaviour and process-induced defects from injection molding of Polyamide 6 with reinforcement of 30 wt% short glass fibers (PA6 GF30) can be predicted and included in the material models for CAE. This will be done through the answering of the following questions.

- What are the defects occurring during the injection molding process (especially when using PA6 GF30 as material)?
- What impact do anisotropy and process-induced weaknesses have on material properties?
- How can anisotropy and process-induced weaknesses be included in material models used for FEA?

Material testing of PA6 GF30 will be performed to capture the anisotropic behaviour of the material. Furthermore, a case study will be performed on the Thule OutWay Hanging bike rack seen in figure 1.1. The two red circles in the figure shows two load bearing consoles produced in PA6 GF30 which is the investigated component. The case study will include component testing, mould fill simulation in Moldex3D, and implementation of material models Mat_157 and Mat_215, which consider fibre orientation, for structural FEA in LS-DYNA.

Figure 1.1: Thule OutWay Hanging bike rack.

1.4 Delimitation

- FEA and MFS will be carried out by personnel at Thule.
- The influences on the mechanical properties will be limited to weld lines, air traps and fibre direction.
- The adaption of production parameters of injection molding to minimize certain defects and obtain wanted fibre direction will not be investigated.

1.5 Ethics and Social Aspects

There are two main aspects to consider regarding ethics and sustainability in this master thesis. The first one is the environmental impact that is caused by the materials used in the products investigated. Are there better alternatives to lower the environmental impact? Since this is not part of the thesis this should not be given much thought. The second, and more important aspect regarding ethics is that the part which will be investigated in the case study is a load bearing part. If this part would break during use, there is a high risk that there would be an accident. Therefore it is of high importance that the material properties and design is chosen correctly.

2

Polymer Materials

Polymer materials are usually divided into thermoplastics and thermosets. When a thermoplastic polymer is heated, it melt into a highly viscous liquid and solidifies when cooled again. This process can be repeated multiple times without a dramatic impact on the properties. In contrary, when a thermoset is heated or mixed with a curing agent, it flows like viscous fluid before chemical cross-linking of the molecules occur. This causes the material to solidify into an infusible mass. Thermoplastics polymers cover around 80 % of the market and are the type that will be investigated further in this master's thesis [1].

2.1 Molecules and Microstructures

Polymers are made up of several smaller units called monomers connected with covalent bonds to form a long single molecule. The majority of all thermoplastic polymers have a carbon chain structure, often with side groups of hydrogen and other organic elements. These polymers are known as hydrocarbon polymers. The simplest variant is called Polyethylene which has a chain of two hydrogen atoms connected to a carbon atom seen in figure 2.1.

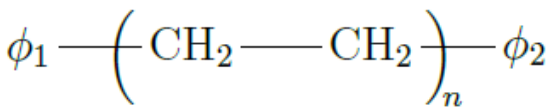

Figure 2.1: Molecular structure of polyethylene.

ϕ_1 and ϕ_2 are the small end groups that do not impact the properties significantly and the n is the number of ethylene monomers the molecule is built from, usually in the order of 10^4.

Polymers are formed in a process called polymerization. There are multiple methods of polymerization, but the resulting polymers fall into two different categories, addition polymers or condensation polymers. Addition polymers are formed through the addition of unsaturated monomers to the end of the growing molecule chain. At the growing end, there is an unpaired electron that attracts the loose monomer. The monomer is attached and the unpaired electron moves to the new end. This process continues until a chain termination reaction occurs which forms a stable

ϕ_2 end group. Condensation polymers are formed through the combination of two often more complex molecules which leaves a residue of a small molecule besides the desired one. This also continues to form a long molecule until the process is stopped [1].

The general idea is that the molecule formed in the polymerization is a long continuous formation. In this case, it is said to be linear. However, it is possible that the chain backbites during polymerization to form a side-branched polymer. Another formation of polymers is called cross-linked polymers. Instead of having a long chain, the monomers in this type connects to multiple other monomers to form a web-like pattern [1]. What type of polymer is formed depends on the process parameters such as monomer type, temperature, pressure, etc. An illustration of the different formations can be seen in figure 2.2.

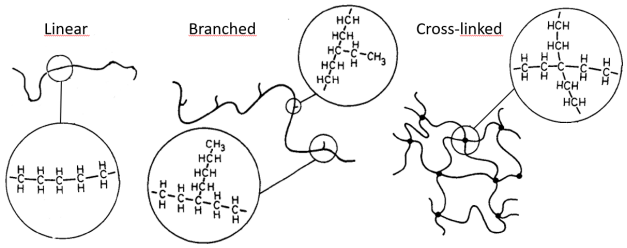

Figure 2.2: Illustration of Linear, Branched, and Cross-linked polymer [1].

If the polymer is composed of two or more different monomers, it is called a copolymer. There are many types of copolymers, such as random, block or graft polymer depending on the order of the different monomers. Generally, the formation of the monomers is random, but when put in order in a linear sequence they are called block copolymer and when one monomer are put in branches it is called graft copolymer. The three types of copolymers are illustrated in figure 2.3.

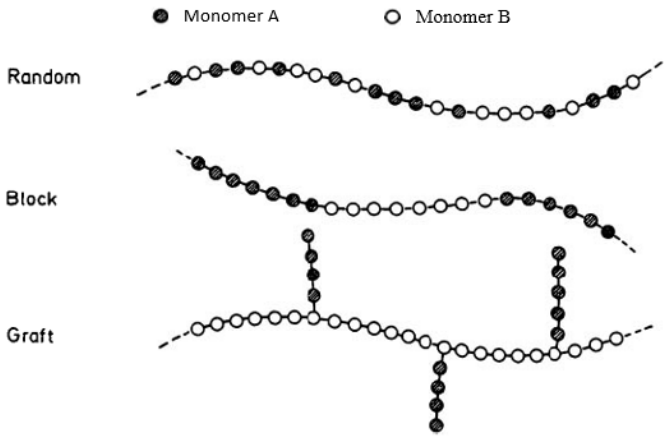

Figure 2.3: Illustration of Random, Block, and Graft copolymer [1].

When the polymers are formed and the temperature is lowered below the melt temperature the melt will start to solidify and form either a crystalline or an amorphous solid. The molecules in an amorphous polymer have a random conformation and are

considered to have no long-range order. Interesting amorphous polymers are considered to be either glasses or elastomers. For a crystalline material, the solidification is known as crystallization which is initiated at nuclei in the melt. Spherulites start to form where the polymer chains fall into an ordered structure. However, between the crystals, amorphous regions are formed which makes crystalline materials also known as semi-crystalline. The proportion of the solid which is crystalline is known as its crystallinity.

The bonds between the polymer chains differs a lot between different polymers. In the amorphous state, the chains can be both chemically cross-linked with covalent or valence bonds or physically through entanglement or being pinned by crystals. In a crystalline state, the chains are bonded together through weaker van der Waals or hydrogen bonds.

2.2 Properties of Polymers

Several properties have to be understood when using polymer material for a component. Using an inappropriate polymer in bad conditions can cause drastic failures.

2.2.1 Temperature Dependency

The properties of thermoplastics are strongly temperature dependent. Depending on if the material is semi-crystalline or amorphous the behaviour differs slightly. There are two temperatures where the behaviour of a polymer material shift drastically, melt temperature T_m and glass transition temperature T_g. The T_g is usually within a span of temperature where the amorphous parts of the material change behaviour. Below the T_g it is in the hard and brittle glassy state. The polymer chains are locked in position by strong bonds which result in high stiffness. When the temperature increases above the T_g the bonds between the chains decreases in strength which makes it possible for them to move relative to one another at applied stress. This is represented by a drop in stiffness. The stiffness relative to the temperature of an amorphous and semi-crystalline material can be seen in figure 2.4.

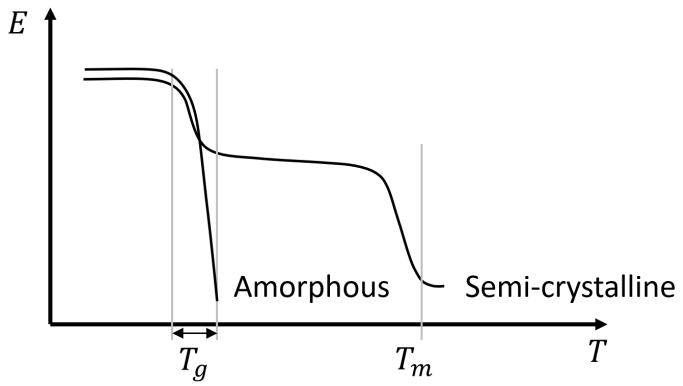

Figure 2.4: Young's modulus versus temperature of an amorphous and a semi-crystalline polymer.

When the temperature reaches T_m the behaviour differs as well. A chemically cross-linked amorphous material will burn, unlike a semi-crystalline material which will melt.

2.2.2 Viscoelasticity

Thermoplastic polymers generally exhibit viscoelastic behaviour meaning that when a force is applied to it, both elastic, plastic and viscous deformation occurs. This behaviour is linked to the movement of the polymer chains relative to each other at an applied load.

The viscoelastic response of thermoplastic, when subjected to stress, is caught by two tendencies, creep and stress relaxation. Creep is what happens when a thermoplastic is subjected to constant stress, but the strain increases with time, which is visualized in figure 2.5. Even if the stress is below the yielding point of the material, plastic deformation occurs due to molecular rearrangement.

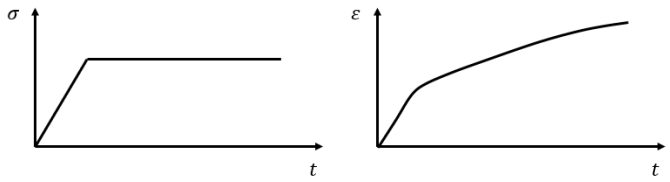

Figure 2.5: Creep visualized as increasing strain at constant stress.

In contrast to creep, stress relaxation occurs when a thermoplastic is subjected to stress to keep the strain constant. Due to the same molecular rearrangement as in creep, the stress to keep the strain is decreasing with time. This is visualized in figure 2.6. Creep and stress relaxation increases with temperature.

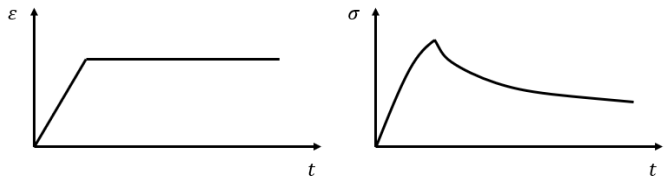

Figure 2.6: Stress relaxation visualized as decreasing stress at constant strain.

Another important factor considering the viscoelastic behaviour of thermoplastics is the reaction to dynamic loading. If a sinusoidal oscillatory strain is applied the stress response of the material will be phase shifted, trailing slightly behind the strain level. This can be described as mechanical damping and is useful to lower vibrations from natural frequencies in construction, in comparison to metals which has non or very low damping effects [1].

2.2.3 Yielding and Fracture

Deformation in polymers differs a lot from metallic materials where plastic deformation is a consequence of dislocation movement. Instead, the deformation in thermo-

plastics is explained by the movement of the molecule chains, such as chain stretch, rotation, slide, and disentanglement [2]. Two typical tensile test curves of a brittle Polystyrene (PS) and a ductile Polyethylene (PE) polymer is shown in figure 2.7. How the material behaves depends on its resistance to yield and to crazing and crack propagation. These mechanisms are affected by surrounding conditions such as temperature, strain rate, type of loading, pressure etc.

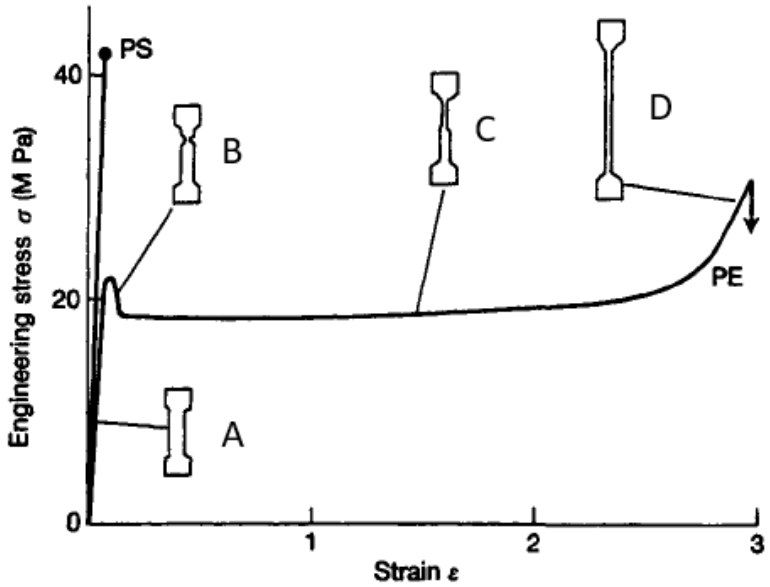

Figure 2.7: Stress versus strain curve from tensile test of PS and PE at room temperature [1].

A, B, C, and D notes four different stages in the deformation process of the ductile thermoplastic PE. During the elastic deformation in step A, the material is stretched without permanent deformation. When the stress reaches the materials yielding point at step B, significant deformation occurs. First, the molecules start to move relative to each other and later the molecules themselves are straightened. The test bars B and C in figure 2.7 visualizes the behaviour of a neck which occurs at yielding and is extended along with the detangle and extension of the molecules. In step D the molecules are fully extended and the stress increases until a macroscopic fracture occurs.

The brittle polymer PS will fracture without significant deviation from the linear-elastic curve. When PS is exposed to high loads crazes are formed from micro-cracks, rendering free surfaces or voids within the material. Craze fibrils are drawn out from the solid part of the polymer until the fracture is reached.

The behaviour of thermoplastic polymers is also highly strain rate dependent according to Eyring's model of solid flow. When a strain is applied, the rate at which it is applied influences the behaviour of the material. A higher strain rate $\dot{\varepsilon}_n$ results in both higher modulus and higher yield stress, but lower total strain due to the shorter time for the molecules to rearrange [1]. This is visualized in figure 2.8.

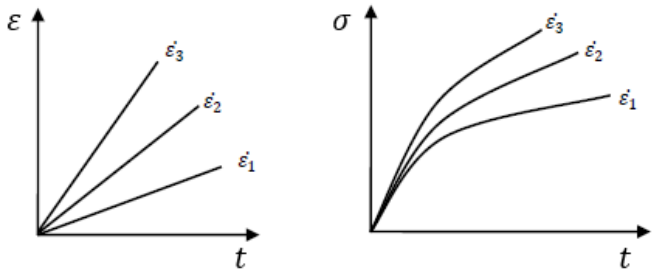

Figure 2.8: Stress and strain curves versus time as recorded from tensile test at room temperature.

In metals, the transition from elasticity to plastic deformation from applied stress is described by mathematical expressions called yielding criterion. The two most common are known as von Mises and Tresca. The yielding of a material is driven by local shear stress whereas fracture is driven by normal stresses. For the Tresca criteria, yielding starts when the maximum shear stress in the material equals the maximum shear stress the material reaches in a regular tensile test. Similarly, for von Mises criteria, yielding starts when the maximum shear energy in the material equals the maximum shear energy the material reaches in a regular tensile test. These assumptions result in two general forms of equations for the Tresca and von Mises criteria respectively.

$$\sigma_{max} - \sigma_{min} = \sigma_y \tag{2.1}$$

$$1/\sqrt{2}[(\sigma_{xx} - \sigma_{yy})^2 + (\sigma_{yy} - \sigma_{zz})^2 + (\sigma_{zz} - \sigma_{xx})^2 + 6(\tau_{xy}^2 - \tau_{yz}^2 - \tau_{zx}^2)]^{1/2} = \sigma_y \tag{2.2}$$

This can be visualized as in figure 2.9.

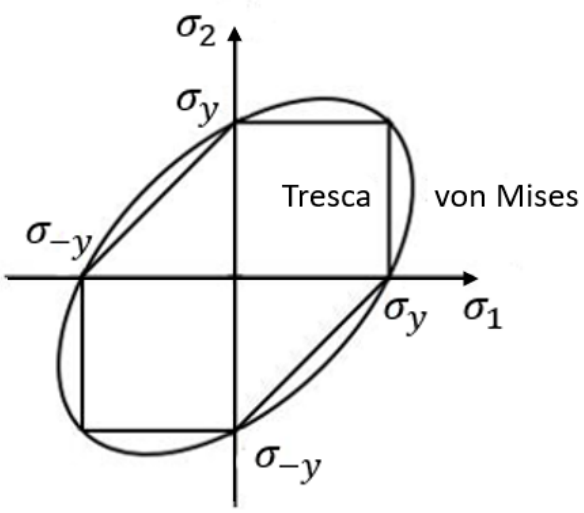

Figure 2.9: Tresca and von Mises yield criterion.

As seen in figure 2.9, the Tresca criteria has a more conservative estimate and will always be less than or equal to von Mises which on the other hand is said to be more accurate [källa].

One thing that is not included in these criteria is the influenced by the hydrostatic component of the stress state. Unlike metals, where this does not need to be included, polymers have shown dependency on hydrostatic pressure. The reason for this is the chain arrangement and deformation micromechanisms of polymers [3] including that it suppresses crazing [1]. Donato and Bianchi [3] have investigated this phenomenon and using one conic and one parabolic modification of the von Mises yield criterion with the introduction of a variable m to account for the unevenness in the tensile and compressive yield strength. The shift towards the negative quadrant seen in figure 2.10 (a) indicates higher yield strength in compressive stress, which is confirmed by results from a tensile and compressive test of PA6 seen in figure 2.10 (b).

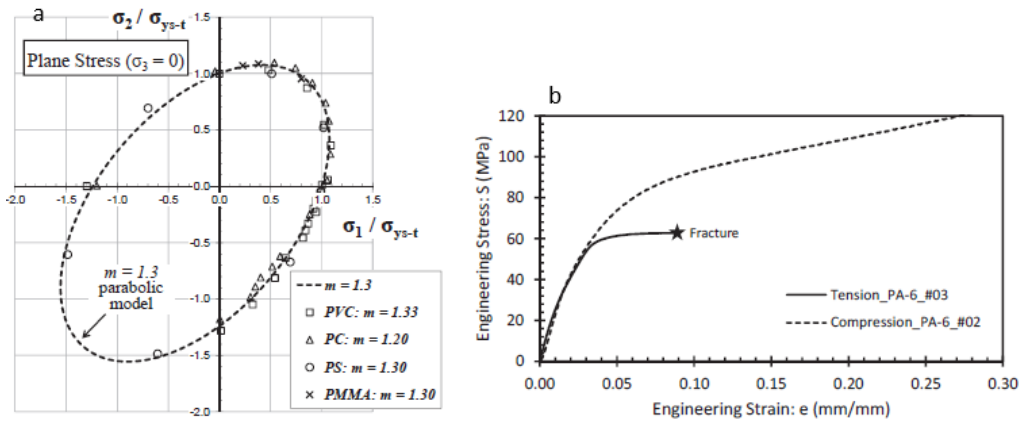

Figure 2.10: (a) Parabolic prediction of von Mises yield criterian at $m = 1.30$ toghether with experimental results of PVC, PC, PS, and PMMA, and (b) tension and compression test of PA6 [3].

2.3 Fiber Reinforced Polymers

Most polymers have a lower density than metals, and strength and stiffness are often not enough for structural load bearing components. By adding reinforcement to a polymer matrix, a light and strong composite material can be obtained. Various types of matrices and reinforcement can be combined to form a composite with the wanted mechanical properties while still preserve the desirable qualities of polymer materials.

The general idea of a fibre reinforced composite is for the polymer matrix to keep the fibres in place and transfer the load between the much stronger and stiffer fibres [1]. In figure 2.11 (a) a polymer matrix reinforced with a single short fibre with length l and diameter d is shown. Figure 2.11 (b) and (c) shows the behaviour of the reinforced matrix and a non reinforced polymer when subjected to a tensile load. The fibre in (b) is stiffer than the matrix causing it to deform less which reduces

the overall strain in comparison to the unreinforced matrix in (c). The strain is visualized by the horizontal lines.

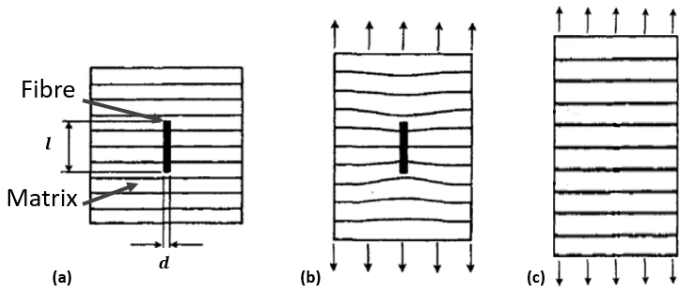

Figure 2.11: A polymer matrix: (a) reinforced with short fibre in undeformed and (b) deformed state, and (c) an unreinforced matrix in deformed state [1].

When adding a sufficient amount of reinforcement the properties of a material changes a lot. As an example, figure 2.12 shows the difference in tensile strength between plain Polyamide 6 (PA6), PA6 reinforced with 5 % montmorillonite platelets (PA6/MMT5), and PA6 reinforced with 25 wt% short glass fibres (PA6/GF25).

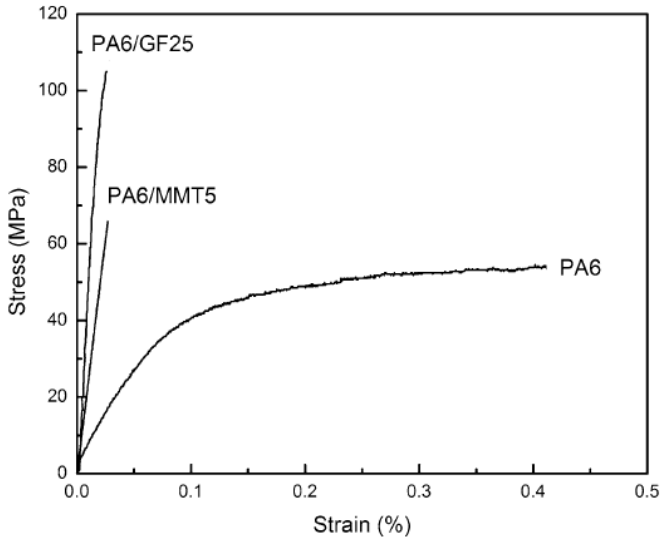

Figure 2.12: Comparison of tensile strength of PA6, PA6/MMT5, and PA6/GF25 [4].

The mechanical performance of short fibre reinforced polymers is affected by several factors. These include fibre and matrix properties, interface characteristics, fibre length distribution, fibre orientation distribution and fibre volume fraction [5], which will be discussed further in the following section.

2.3.1 Reinforcement Materials

As mentioned, there are several types of reinforcement materials, including particles, flakes, whiskers, short fibres, continuous fibers and sheets, where the last three mentioned are most common in combination with a polymer matrix [6]. Concerning

fibres, there are many natural, such as cotton, jute, hemp, sisal and ramie. However, industrial fibers with higher strength and stiffness have been developed for high demand applications. This includes glass fibres, carbon fibres, aramid fibres and other polymeric fibres. The properties of some fibres are shown in table 2.1.

Table 2.1: Density, Elongation, Tensile strength and Young's modulus of some fibre materials [7] [1].

Fibre	Density (g/cm^3)	Elongation (%)	Tensile Strength (MPa)	Young's Modulus (GPa)
Carbon	1.66-2.25		2500-4500	230-340
Aramid	1.4	3.3–3.7	3000–3150	63–67
Glass	2.5	2.5–3	2000–4570	70-86
Cotton	1.5–1.6	3–10	287–597	5.5–12.6
Hemp	1.48	1.6	550–900	70
Jute	1.3–1.46	1.5–1.8	393–800	10–30
Ramie	1.5	2–3.8	220–938	44
Sisal	1.33–1.5	2–14	400–700	9–38

Glass fibres are further divided depending on the chemical composition and specific usage. Most glass fibres are silica-based with around 60 wt.% SiO_2, in a combination of other oxides from aluminium, calcium, magnesium, sodium, potassium, and boron for example. Three common glass fibres are E glass, C glass and S glass, named after their specific characteristics. E glass is a good electrical insulator, C glass has good corrosion resistance and S contains a lot of silica which make it withstand high temperatures. E glass also has relatively high strength and stiffness making it the most used glass fibre [6].

One conventional way of producing E glass is to put the wanted mix of raw materials in a hopper where it is melted. The molten glass is fed into bushings or crucibles each containing about 200 wholes which the molten glass flow through to form continuous filaments. The filaments are gathered into a strand which is wound on a drum [6].

2.3.2 Polymer Matrix Materials

Polymer matrices can be divided into the two categories mentioned in the previous chapter, thermoset and thermoplastic. Thermoset resins are often used together with sheet laminates and long fibres for small batches using production methods such as hand lay-up, bag moulding, pultrusion or filament winding [6]. This can include the production of boat hulls, kayaks, rods, wind turbine blades and other components of similar shape. On the other hand, thermoplastic matrices are more often used in various moulding techniques, especially injection moulding usually using short fibre reinforcement for larger batches.

Some common thermoplastics used as a matrix in composites are Polyamide (PA), Polypropylene (PP), Polyethylene (PE), Polyethylene terephthalate (PET), Polylactic acid (PLA), Polyurethane (PU), Polyethersulfone (PES), Polycaprolactone (PCL) [7][1].

2.3.3 Fibre/Matrix Interface

When designing composite materials it is important to consider not only the reinforcement and matrix material individually but also the interaction between their surfaces. This is called the interface. Even if the reinforcement is usually very small in dimensions the high content results in a large internal surface area which means that the properties of the interface region are extremely important. The two most important factors to consider in fibre reinforced polymers are wettability and the type of bonding. Furthermore, it is also important to consider the impact of factors such as temperature, diffusion, residual stresses, and so on.

Wettability is described as the ability of a liquid to spread on a solid surface. Usually described by a drop placed on a solid surface where the contact angle is measured, or calculated from specific surface energies. This concept assumes a perfectly smooth surface of the solid which of course is not true in practice. The interface between fibre and matrix is rather rough which means that the matrix must have a good wettability to form an intimate contact. However, good wettability does not necessarily result in a strong bond at the interface.

Bonding at the interface can be classified as mechanical, physical or chemical. Mechanical bonding can be described as keying or interlocking generating friction between the two surfaces. Physical bonding includes week, secondary and van der Waals forces, dipolar interactions and hydrogen bonding. Chemical bonding is achieved when there is a diffusion process of atomic or molecular transport occurring. This can include the formation of a solid solution resulting in a thickness of the interface region.

To achieve a good interface in glass fiber reinforced polymers (GFRP), the fibres are the first surface treated with a so called size after production to protect them from inducing surface defects. Before the fibres are combined with the polymer matrix, the size is removed and a coupling agent is added to enhance bonding at the interface. Usually, an organosilane compound is used which includes a silicon base with one side group compatible with the matrix and another compatible with the fibre [6]. This has been described as a chemical bridge and can be visualized as in figure 2.13, where R is the matrix compatible group and M is the fibre compatible group.

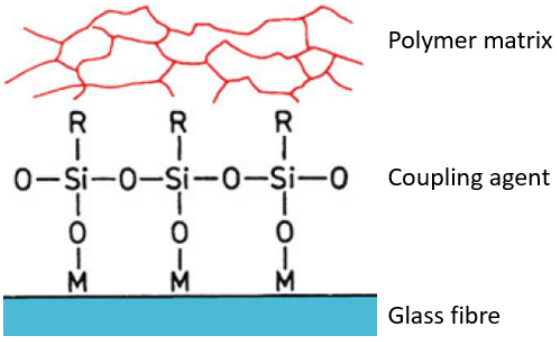

Figure 2.13: Chemical bridge between matrix and fibre using organosilane coupling agent [6].

This chemical generates a strong bond at the interface. However, if the interface is too strong it will generate a material with low toughness due to the initiation of cracks at the interface region. In contrary, a week interface will behave like a fibre bundle relying only on inter-fibre friction resulting in lower strength. An optimum interface will generate a both strong and tough composite with multiple failure sites spread over the whole interfacial area.

2.3.4 Micro-mechanics of GFRP

The micro-mechanical approach of composites includes the analysis of the constituents individually. Hence, there has to be a knowledge about the geometrical arrangement of the fibres. Generally, the properties of a fibre reinforced polymer can be described by the rule of mixture, first described by Voigt. This combines the properties of the matrix (the viscoelasticity is neglected) and the reinforcement in an isostrain or action-in-parallel situation.

$$P_c = fP_f + (1 - f)P_m \tag{2.3}$$

P is the investigated property of the composite (c), the fibre (f), and the matrix (m), and f is the volume fraction of fibres. Note that fibre fraction often is measured in weight as well. The rule of mixture generally works for properties such as Young's modulus, Tensile strength, density and so on. This assumes a matrix reinforced with uniaxially aligned continuous fibres which are perfectly adhered to the matrix and having the same Poisson's ratio, causing them to undergo the same elongation. For loads in the transverse direction, there is a situation called isostress or action-in series instead, where a similar model developed by Reuss (1929) is used [6].

$$1/(P_c) = f/(P_f) + (1 - f)/(P_m) \tag{2.4}$$

The longitudinal (E_1) and transverse (E_2) Young's modulus of a composite can then be plotted against the volume fraction of fibres according to figure 2.14.

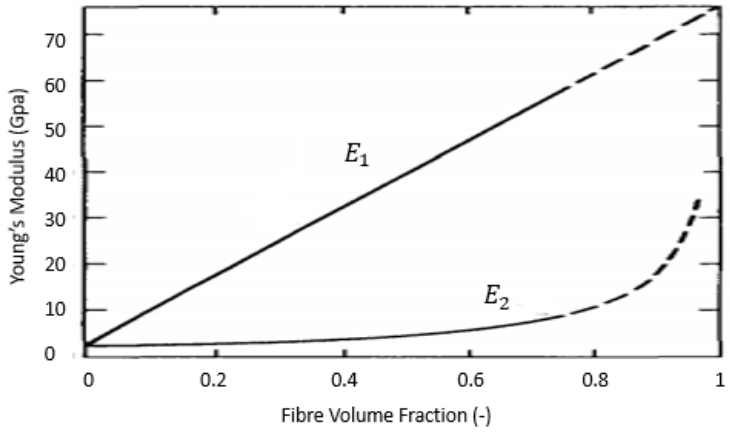

Figure 2.14: Young's modulus of a glass-fibre reinforced polymer predicted by rule of mixture [1].

As seen, E_1 is mainly dependent och the fibre modulus and the polymer matrix mainly works as a glue to keep the fibres together whereas E_2 is mainly dependent on the polymer matrix. This type of composite is known as unidirectional, which is good when the load needs to be carried in only one direction. Commonly, multiple layers of unidirectional fibre composites at different angles are used to get a stiffer and stronger material in multiple directions, but due to manufacturing factors, this is not always possible. Therefore short fibre reinforced polymers are often used, but then a modified rule of mixture needs to be used [5].

$$P_c = XfP_f + (1 - f)P_m \tag{2.5}$$

X is a coefficient including factors such as the fibre aspect ratio, fibre orientation, and fibre-matrix adhesion depending on which property is included [5]. The fibre aspect ratio (AR) is simply

$$AR = l/d \tag{2.6}$$

l is the fibre length and d is the fibre diameter. The fibre length in a short fibre reinforced polymer (SFRP) is highly dependent on the production method. In the process of injection moulding, the fibres will break due to shear stresses exerted by the screw. This will cause a distribution of fibre lengths depending on the process parameters and matrix viscosity. The injection moulding process will be further discussed later. There is a critical aspect ratio where the critical fibre length l_c notes the length of a fibre where it no longer can carry full load.

Similarly, the fibre orientation distribution is highly dependent on the processing parameters, but also mould geometries. When a large mould is filled, the fibres tend to orient themselves creating a skin-core-skin structure [5]. As seen in figure 2.15 the fibres in the core layer are mainly oriented transverse to the melt flow direction (MFD), whereas the fibres in the skin layers are mainly oriented along the MFD. On the contrary, in a thin specimen, the fibres will mainly be aligned along the MFD [5].

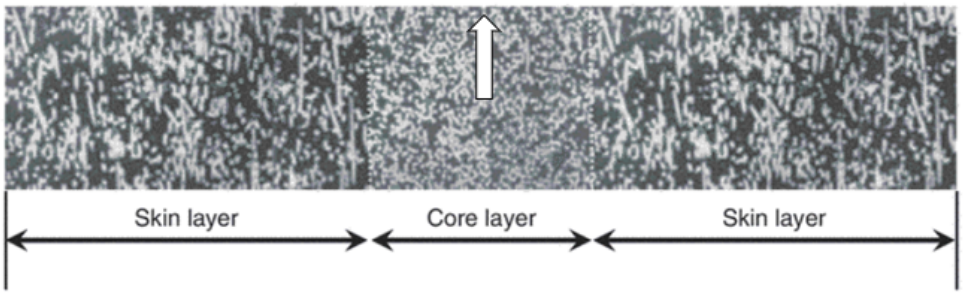

Figure 2.15: Microscopic image of the skin-core-skin structure. The white arrow denotes the MFD [5].

The recently mentioned rules of mixtures do not really capture the complexity of fibre reinforced materials. Therefore the mechanical behaviour of composites has

been described further. The state of stress and strain can be described by six independent components. These include three tensile and three shear components. To describe the stress and strain relation of an anisotropic body with no symmetry, 21 independent elastic components is required. On the contrary, an elastically isotropic body only need two independent elastic constants [6]. It can be understood that the symmetry of the material determines the number of elastic constants needed for a material. However, there are more accurate ways of obtaining these constants including the consideration of the inevitable scatter of fibre distribution. If there the fibres are short and aligned in the loading direction, there are numerical equations, called Halpin-Tsai equations, that can be used to predict the elastic constants [6]. A general form of the equations are

$$p/p_c = (1 + \xi\eta V_f)/(1 - \eta V_f) \tag{2.7}$$

where

$$\eta = (p_f/p_m - 1)/(p_f/p_m + \xi) \tag{2.8}$$

p represent one of the investigated moduli, p_f and p_m are the corresponding moduli of the fibre and matrix, V_f is the volume fraction of fibres, and ξ is a measure of the reinforcement that depends on fibre geometry, fibre distribution, and loading conditions.

Mori and Tanaka developed a method known as the Mori-Tanaka model to determine the effective stiffness of composite materials [8]. A simplified derivation of the model can be described as

$$\bar{C} = C^m + V_f[C^f - C^m]B \tag{2.9}$$

$$B = T(V_m I + V_f T)^{-1} \tag{2.10}$$

$$T = [I - PC^{m-1}(C^m - C^f)]^-1 \tag{2.11}$$

$\bar{C}$ is the effective stiffness tensor of the composite, C^m and C^f is the related stiffness tensors of the matrix and the fibre. B is the strain concentration tensor that relates the homogenized strain in the fibre to strain due to remote stress. T relates the elastic properties of the fibre and the matrix according to Eshelby inclusion model, where P is Eshelby's tensor which relates eigenstrain with strain [8]. The final form of the Mori-Tanaka model-based homogenized elastic tensor $\bar{C}$ can then be presented as

$$\bar{C} = C^m + V_f[C^f - C^m][I - PC^{m-1}(C^m - C^f)]^{-1}(V_m I + V_f T)^{-1} \tag{2.12}$$

Eshelby's inclusion model is based on an ellipsoidal inclusion in an infinite matrix visualized in figure 2.16. This model is as mentioned used to calculate the stress and strain fields around the inclusion [5].

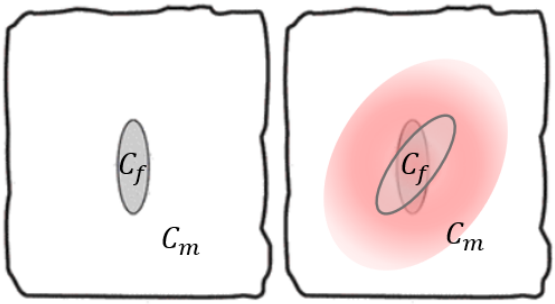

Figure 2.16: Visualization of Eshelby's inclusion model.

2.3.5 Macro-mechanics of GFRP

As mentioned in the previous section composites are often laminates bonded together and oriented such as mechanical and physical properties are different in different directions, known as an anisotropic material. For a macro-mechanical analysis of a composite lamina, information from the micro-mechanical analysis is used as input. When this is done, it is possible to treat the material as homogeneous, orthotropic sheets. It is then possible to use the well-established theory of laminated plates to analyze the composite [6]. This is to some extent also valid for SFRP since they can be simulated as various laminates with different fibre angle orientations [5].

When a cube is exposed to a load, the stresses in the cube can be described three normal and six shear components, σ_{ij} (where i, j=1, 2, 3), acting on the faces of the cube. This stress cube is visualized in figure 2.17. The subscript i refers to the outward direction normal to the face at which the stress acts, and j refers to which direction the stress acts.

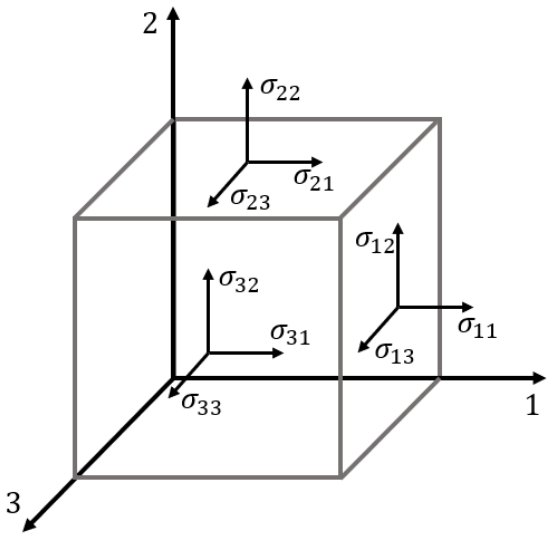

Figure 2.17: A three dimensional cube with stress components when exposed to a normal force.

Each stress component has a corresponding strain ε_{ij} which together with a stiffness forms the generalised Hooke's law for anisotropic materials.

$$\sigma_{ij} = C_{ijkl}\varepsilon_{kl} \quad i,j,k,l = 1,2,3 \tag{2.13}$$

σ_{ij} is the stress tensor, ε_{kl} the strain tensor, and C_{ijkl} is the stiffness tensor. This equation represents nine equations where the stiffness tensor has 9x9 elements.

$$\begin{bmatrix}\sigma_{11}\\ \sigma_{22}\\ \sigma_{33}\\ \sigma_{23}\\ \sigma_{31}\\ \sigma_{12}\\ \sigma_{32}\\ \sigma_{13}\\ \sigma_{21}\end{bmatrix} = \begin{bmatrix} C_{1111} & C_{1122} & C_{1133} & C_{1123} & C_{1131} & C_{1112} & C_{1132} & C_{1113} & C_{1121} \\ C_{2211} & C_{2222} & C_{2233} & C_{2223} & C_{2231} & C_{2212} & C_{2232} & C_{2213} & C_{2221} \\ C_{3311} & C_{3322} & C_{3333} & C_{3323} & C_{3331} & C_{3312} & C_{3332} & C_{3313} & C_{3321} \\ & & & & & & & & \\ & & & & & & & & \\ & & & & & & & & \\ & & & & & & & & \\ C_{2111} & C_{2122} & C_{2133} & C_{2123} & C_{2131} & C_{2112} & C_{2132} & C_{2113} & C_{2121} \end{bmatrix} \begin{bmatrix}\varepsilon_{11}\\ \varepsilon_{22}\\ \varepsilon_{33}\\ \varepsilon_{23}\\ \varepsilon_{31}\\ \varepsilon_{12}\\ \varepsilon_{32}\\ \varepsilon_{13}\\ \varepsilon_{21}\end{bmatrix} \tag{2.14}$$

Note that the shear stresses and strains ($i \neq j$) often are written as τ_{ij} and γ_{ij}. A contracted notation can be used to reduce the number of subscripts. Thus, the stress-strain relationship can be written as.

$$\sigma_i = C_{ij}\varepsilon_j \quad i,j = 1,2,3...,6 \tag{2.15}$$

with the following matrix notation.

$$\begin{bmatrix}\sigma_1\\ \sigma_2\\ \sigma_3\\ \sigma_4\\ \sigma_5\\ \sigma_6\end{bmatrix} = \begin{bmatrix} C_{11} & C_{12} & C_{13} & C_{14} & C_{15} & C_{16} \\ & C_{22} & C_{23} & C_{24} & C_{25} & C_{26} \\ & & C_{33} & C_{34} & C_{35} & C_{36} \\ & & & C_{44} & C_{45} & C_{46} \\ & & & & C_{55} & C_{56} \\ & & & & & C_{66} \end{bmatrix} \begin{bmatrix}\varepsilon_1\\ \varepsilon_2\\ \varepsilon_3\\ \varepsilon_4\\ \varepsilon_5\\ \varepsilon_6\end{bmatrix} \tag{2.16}$$

By doing this the stiffness constants can be reduced from 81 to 36 elastic constant. Furthermore, the symmetry along the diagonal results in the 21 independent elastic constants mentioned in the previous section about micro-mechanics.

Usually, a converse notation is used including a compliance matrix S_{ij}, which is the inverse of the stiffness matrix.

$$\varepsilon_i = S_{ij}\sigma_j \tag{2.17}$$

For most materials, the elastic constants can be reduced further through the consideration of symmetry. As mentioned, a fully isotropic material where the elastic properties are independent of direction, only C_{11} and C_{12} are independent. This is because Young's modulus E, Poisson's ratio v, shear modulus G, and bulk modulus K are all interrelated.

$$E = 2G(1+v) \quad and \quad K = E/(3(1-2v) \tag{2.18}$$

This results in the following equation using the compliance matrix.

$$\begin{bmatrix} \varepsilon_1 \\ \varepsilon_2 \\ \varepsilon_3 \\ \varepsilon_4 \\ \varepsilon_5 \\ \varepsilon_6 \end{bmatrix} = \begin{bmatrix} S_{11} & S_{12} & S_{12} & 0 & 0 & 0 \\ & S_{11} & S_{12} & 0 & 0 & 0 \\ & & S_{11} & 0 & 0 & 0 \\ & & & 2(S_{11}-S_{12}) & 0 & 0 \\ & & & & 2(S_{11}-S_{12}) & 0 \\ & & & & & 2(S_{11}-S_{12}) \end{bmatrix} \begin{bmatrix} \sigma_1 \\ \sigma_2 \\ \sigma_3 \\ \sigma_4 \\ \sigma_5 \\ \sigma_6 \end{bmatrix} \tag{2.19}$$

Looking at a laminated composite the situation is different. Here a plane stress condition is assumed, causing the through-thickness stress components to be zero. This results in a reduced class of anisotropy called orthotrophy. Due to the symmetry, the number of elastic constants is reduced in comparison to a fully anisotropic material. Hence, for an orthotropic material, the compliance matrix is written as.

$$\begin{bmatrix} S_{ij} \end{bmatrix} = \begin{bmatrix} S_{11} & S_{12} & S_{13} & 0 & 0 & 0 \\ & S_{22} & S_{23} & 0 & 0 & 0 \\ & & S_{33} & 0 & 0 & 0 \\ & & & S_{44} & 0 & 0 \\ & & & & S_{55} & 0 \\ & & & & & S_{66} \end{bmatrix} \tag{2.20}$$

For example, the elastic constants of a 50 wt% carbon fibre reinforced epoxy vary with the fibre directions according to figure 2.18.

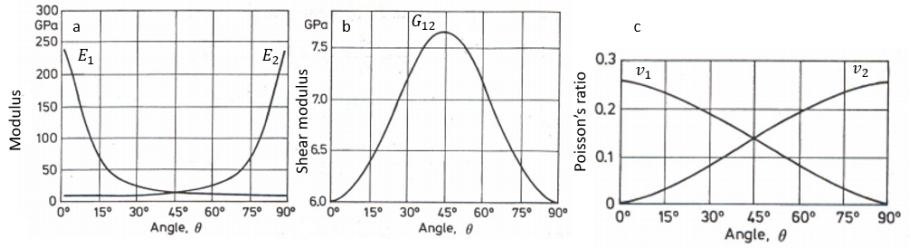

Figure 2.18: Variation of elastic constants (a) Young's modulus, (b) Shear modulus, and (c) Poisson's ratio depending on fibre orientation in a 50 wt% carbon fibre reinforced epoxy .

2.3.6 Strength and Fracture of GFRP

Similarly to the elastic properties of fibre reinforced composites, the strength can be described in multiple ways. When the ultimate stress is reached in a unidirectional lamina, there are typically three ways in which the failure occurs. Those are by axial tensile stress, transverse tensile stress, and shear stress, illustrated in figure 2.19.

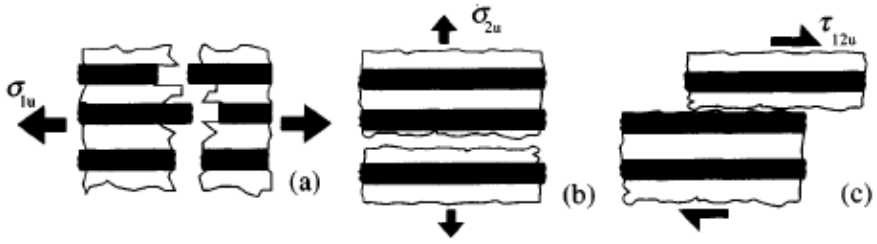

Figure 2.19: Illustration of failure from (a) axial tensile stress σ_{1u}, (b) transverse tensile stress σ_{2u}, and (c) shear stress τ_{12u} [9].

Furthermore, for axial tensile failure, several modes are describing how failure occurs, mainly depending on the loading conditions, fibre and matrix, and the interface between them. For a fibre reinforced polymer, the matrix material usually has a higher strain at fracture than the fibre [6]. If the following condition is met, the composite will show a single fracture since the matrix will not be able to carry additional load as the fibres are breaking.

$$\sigma_{fu}V_f > \sigma_{mu}V_m - \sigma'_m V_m \tag{2.21}$$

σ'_m is the matrix stress corresponding to the fibre fracture strain and σ_{fu} and σ_{mu} are the ultimate tensile stresses of the fibre and the matrix respectively. V_f and V_m is the fibre and matrix volume fraction respectively. If the following condition is met instead, the fibres will break in multiple places until the matrix fractures.

$$\sigma_{fu}V_f < \sigma_{mu}V_m - \sigma'_m V_m \tag{2.22}$$

These conditions are plotted in figure 2.20 which shows the strength versus the volume fraction of fibres. Left of the cross-over point, single fracture occurs whereas multiple fractures occurs on to right.

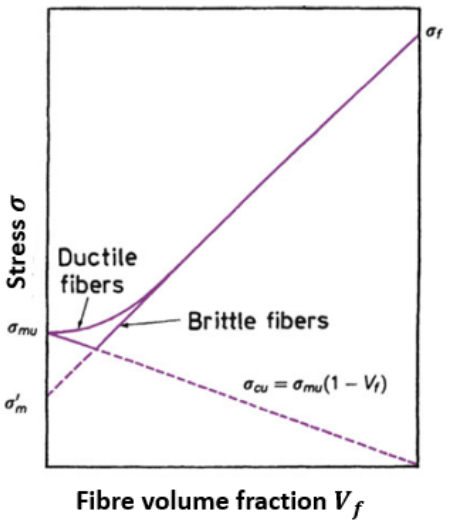

Figure 2.20: Strength of a composite versus the fibre volume fraction of a composite with fibres having lower fracture strain than the matrix [6].

The modes at which the fracture of a fibre reinforced polymer occurs are commonly observed to be debonding of the fibre/matrix interface, fibre pullout and delamination fracture. Generally, some fibre pullout occurs at fracture, which will produce shear stresses parallel to the fibres, increasing the toughness. However, to obtain maximum tensile strength, it is wanted that the fibre break rather than being pulled out from the matrix. Figure 2.21 shows a visualisation of fibre pull out and debonding at a crack.

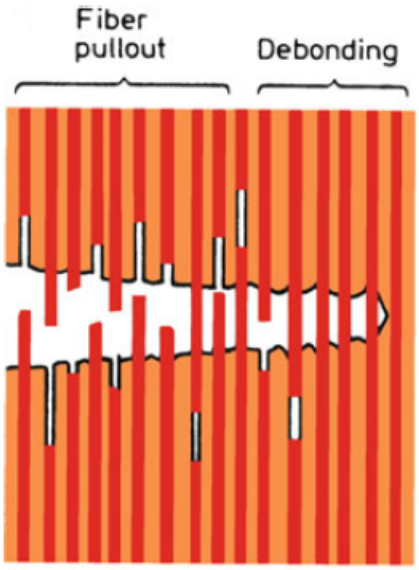

Figure 2.21: Fibre pullout and debonding at a crack [6].

To further describe the strength of a short fibre reinforced composite, there is a model called the shear lag model developed by Cox. It describes the stress transformation in a composite with straight and aligned fibres. The model assumes that the tensile

stress at the fibre ends is small, less or equal to the matrix stress, hence no stress is transferred at the ends. If the matrix has a linearly elastic (a) or elastic-plastic (b) behaviour has some impact on the final properties as seen in figure 2.22 [5].

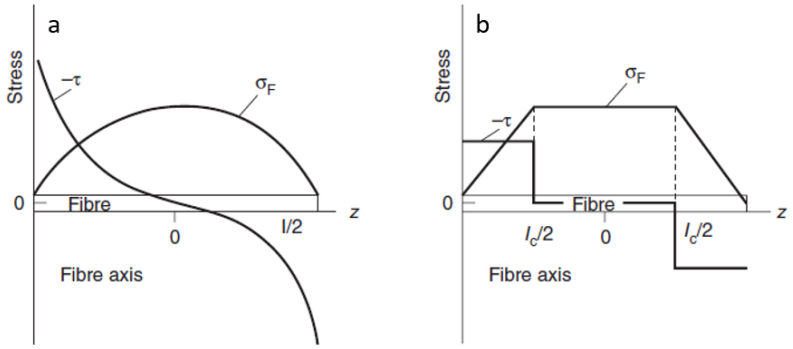

Figure 2.22: Tensile (σ_F) and shear stress (τ) distribution along the length (l) and critical length (l_c) of a short fibre in an (a) linearly elastic and an (b) elastic-plastic matrix [5].

For the ideal case with elastic components and bonded interface, it is assumed that no stress is transferred at the end of the fibres, but close to the end, there will be small stresses. Since the fibres are stiffer than the matrix there are deviations in the mean displacement and shear stresses along the interface are built up. The load is transferred to the fibre until the stress corresponding to a continuous fibre composite is reached. For an elastic-plastic matrix, the fibre stress is determined by the constant shear stress of the matrix in the plastic state. For both cases, the fibres are not fully loaded which lowers the reinforcement efficiency compared to continuous fibre reinforcement. As mentioned before, the critical fibre length (l_c) is important when looking at the fibre length effects [5]. The prediction of the stress in the fibre (σ_f) along the fibre length x is described by Cox according to the following equation [1].

$$\sigma_f = E_f \varepsilon_f \left\{ 1 - \left[\frac{\cosh(na\frac{2x}{l})}{\cosh(na)} \right] \right\} \tag{2.23}$$

E_f is the Young's modulus of the fibre, a is the fibre aspect ratio, l is the fibre length, and n is a dimensionless constant determined by the following equation [1].

$$n = \sqrt{\left[\frac{2G_m}{E_f} \ln(2R/d) \right]} \tag{2.24}$$

G_m is the shear modulus of the matrix, 2R is the distance from the fibre to its nearest neighbour, and d is the fibre diameter. The shear stress at the interface (τ_i) is obtained by differentiating equation 2.25.

$$\tau_i = \frac{n}{2} E_f \varepsilon_1 \frac{\sinh(na\frac{2x}{l})}{\cosh(na)} \tag{2.25}$$

By inspecting the cox equation it can be concluded that the aspect ratio along with n has a high impact on the stresses of the fibre and the interface.

To describe the failure of fibre reinforced composites under multiaxial in-plane loading, several strength (or failure) criterion have been proposed. Some of the most used are the maximum stress criterion, the maximum strain criterion, the maximum work (or the Tsai-Hill) criterion, and the quadratic interaction (or the Tsai-Wu) criterion [6][9][10].

The maximum stress criteria simply postulate that failure will occur when the stress in the material exceeds the corresponding ultimate strength. This includes the ultimate tensile and compression strength in the fibre direction and transverse to the fibre direction along with the ultimate shear stress [6][9][10]. Equations for each failure can be obtained. For tensile loading, these look like

$$\sigma_{xu} = \sigma_{1u} / \cos^2 \Phi \tag{2.26}$$

$$\sigma_{xu} = \sigma_{1u} / \sin^2 \Phi \tag{2.27}$$

$$\sigma_{xu} = -\tau_{12u} / \cos \Phi \sin \Phi \tag{2.28}$$

σ_{xu} is the failure stress, σ_{1u}, σ_{2u}, and τ_{12u} is the ultimate strength in longitudinal, transverse and shear direction, and Φ is the angle of which the stress is applied relative to the fibre direction. For a lamina with 50% glass fibre, the prediction of failure according to these equations can be plotted as in figure 2.23 [9].

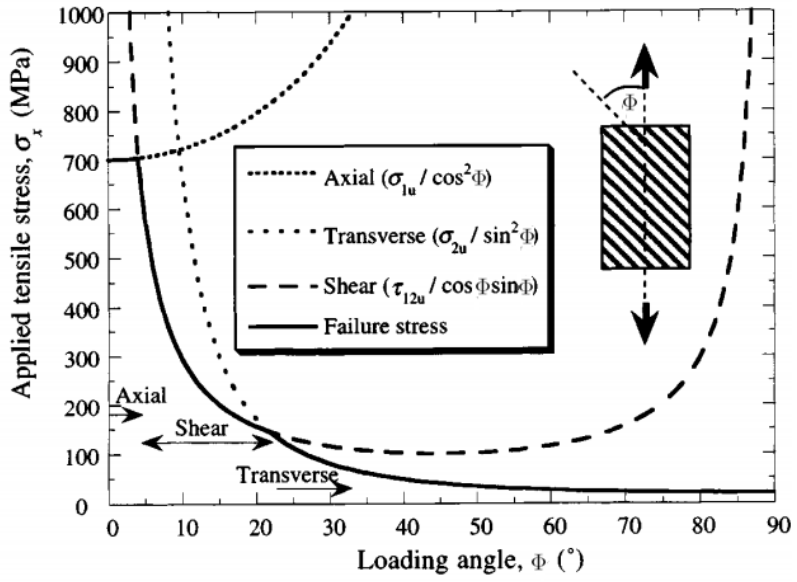

Figure 2.23: Prediction of failure of a lamina with 50 % GF according to maximum stress criteria [9].

The maximum strain criterion similarly postulates that failure occurs when the strain exceeds the corresponding ultimate strain. Both maximum stress and strain criterion are not satisfactory since they do not include any interaction of failure modes [9].

The Tsai-Hill criterion origins from Hill's yield criterion which in turn origins from the von Mises criterion. Hill's yield criterion is a generalization of von Mises used for orthotropic materials and described by the following equation [11].

$$\begin{aligned} f = F(\sigma_{22} - \sigma_{33})^2 + G(\sigma_{33} - \sigma_{11})^2 + (\sigma_{11} - \sigma_{22})^2 + L(\sigma_{23}^2 + \sigma_{32}^2) \\ + M(\sigma_{13}^2 + \sigma_{31}^2) + N(\sigma_{12}^2 + \sigma_{21}^2) - 1 \end{aligned} \tag{2.29}$$

F, G, H, L, M, and N are constants obtained by material testing in different orientations and derived by the following equations.

$$F = \frac{1}{2}\left(\frac{1}{R_{22}^2} + \frac{1}{R_{33}^2} - \frac{1}{R_{11}^2}\right) \tag{2.30}$$

$$G = \frac{1}{2}\left(\frac{1}{R_{33}^2} + \frac{1}{R_{11}^2} - \frac{1}{R_{22}^2}\right) \tag{2.31}$$

$$H = \frac{1}{2}\left(\frac{1}{R_{11}^2} + \frac{1}{R_{22}^2} - \frac{1}{R_{33}^2}\right) \tag{2.32}$$

$$L = \frac{3}{2R_{23}^2} \tag{2.33}$$

$$M = \frac{3}{2R_{13}^2} \tag{2.34}$$

$$N = \frac{3}{2R_{31}^2} \tag{2.35}$$

R_{ij} is the anisotropic ratios described by the following general equation.

$$R_{ij} = \frac{\sigma_{y,ij}}{\sigma_{y,ref}} \tag{2.36}$$

$\sigma_{y,ij}$ is the yield strength in the corresponding test direction and $\sigma_{y,ref}$ is the yield stress in the reference direction, 11 [11].

The Tsai-Hill is instead used when behaviour is different in tension and compression and postulates that failure occurs when the distortion strain energy is exceeded.

This is described as the following equation for a transversely isotropic orthotropic material [6][9][10].

$$(\sigma_1/\sigma_{1u})^2 + (\sigma_2/\sigma_{2u})^2 - \sigma_1\sigma_2/\sigma_{1u}^2 + (\tau_{12}/\tau_{12u})^2 = 1 \tag{2.37}$$

Compared to the previous two criteria, the Tsai-Hill criterion considers the interaction between failure modes. However, there is no distinction between tensile and compressive stress which is of importance as already discussed. To take the tensile and compressive stress into account, modifications have been done to form the Tsai-Wu criterion [6][9][10].

$$F_1\sigma_1 + F_2\sigma_2 + F_{11}\sigma_1^2 + F_{22}\sigma_2^2 + F_{66}\sigma_6^2 + 2F_{12}\sigma_1\sigma_2 = 1 \tag{2.38}$$

All F ar strength parameters, where F_1 and F_{11} are determined by longitudinal tensile and compressive tests, F_2 and F_{22} determined by transverse tensile and compressive tests, F_{66} is determined by longitudinal shear tests, and F_{12} is a determined by biaxial testing. Figure 2.24 shows a comparison of the four described criteria [10].

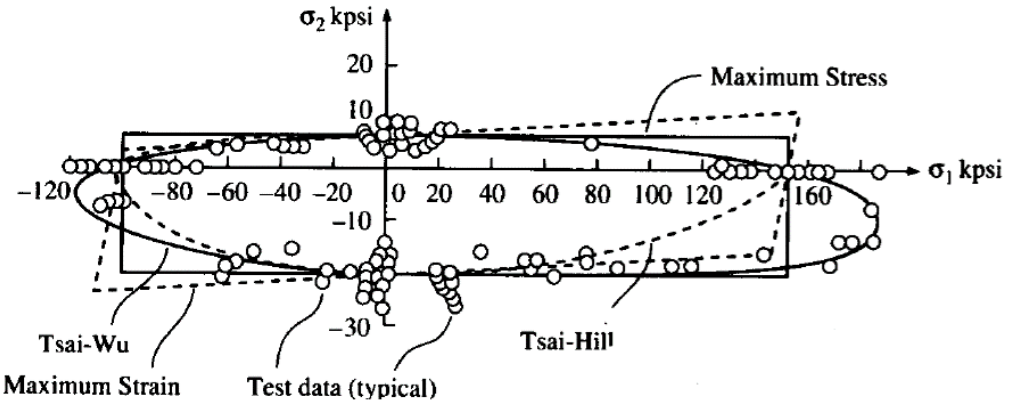

Figure 2.24: Comparison of the four described failure criteria [10].

2.4 Polyamide 6 GF30

Polyamide (PA) is family of polymers including an amide group built from the combination of Oxygen (O) and Nitrogen (N) together with carbon and hydrogen atoms. Due to its excellent properties, Polyamide is one of the most widely used polymers in engineering where it is more commonly known as Nylon [1]. There are various kinds of Polyamides which are depending on the shape and length of the repeating unit, the monomer. Aliphatic Polyamides have a linear configuration, hence they are semi-crystalline. Polyamide 66 (PA66) was the first one to be developed and used in 1938 as a fibre. Polyamide 6 (PA 6) were introduced in 1946 and is produced through ring-opening of Caprolactam [12]. This reaction is presented in figure 2.25.

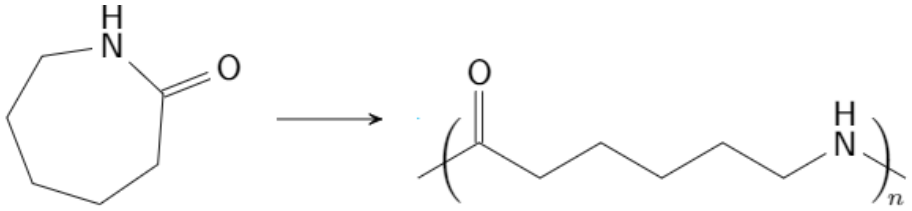

Figure 2.25: Ring opening of Caprolactam to form PA 6.

Other commonly used polyamides are PA11, PA12, PA46, PA69, PA610, and PA612 [1][12]. Some of the wanted properties of Polyamides are their fast crystallization, chemical resistance, toughness, lubricity, fatigue resistance, and mechanical strength [12]. However, due to the molecular formation including CO and NH groups, Polyamides are very prone to absorb water (H_2O). The water molecule bond to the polymer through these groups which causes the material properties to change. Test have shown that the PA6 absorbed 2.7 and 9.5 % water in weight when exposed to 50 and 100 % relative humidity (RH) respectively [1]. Figure 2.26 visualize how the water molecules interact with the PA 66 polymer.

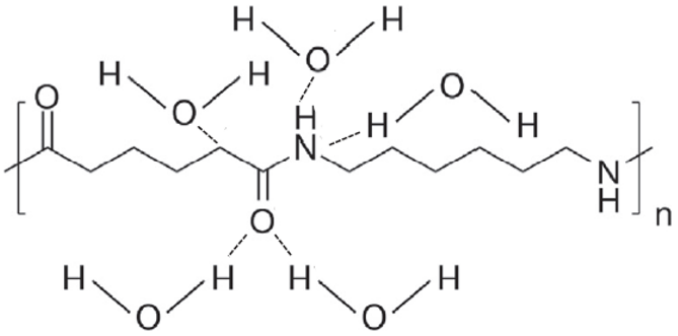

Figure 2.26: Interaction between water molecules and a PA 66.

To increase the mechanical properties of PA 6 it is common to reinforce it with glass fibre. This increases the strength and stiffness which makes it a suitable substitution for metals in structural component to lower the weight.

Several authors have investigated the effect of water absorption on the mechanical properties of Polyamide materials with and without adding of fibre reinforcements. Chaichanawong et. al. [13] investigated how water influenced ultimate tensile strength, modulus of elasticity, elongation, yield strength, and flexural strength of PA 66 with different content of short glass fibre reinforcement (0 wt%, 10 wt%, 20 wt%, and 30 wt%). Specimens were immersed in distilled water for 0 to 60 days with a subsequent tensile test and measurement of moisture content. The results are presented in figure 2.27 which indicates that the biggest changes in mechanical properties occur during the first 7 days in water.

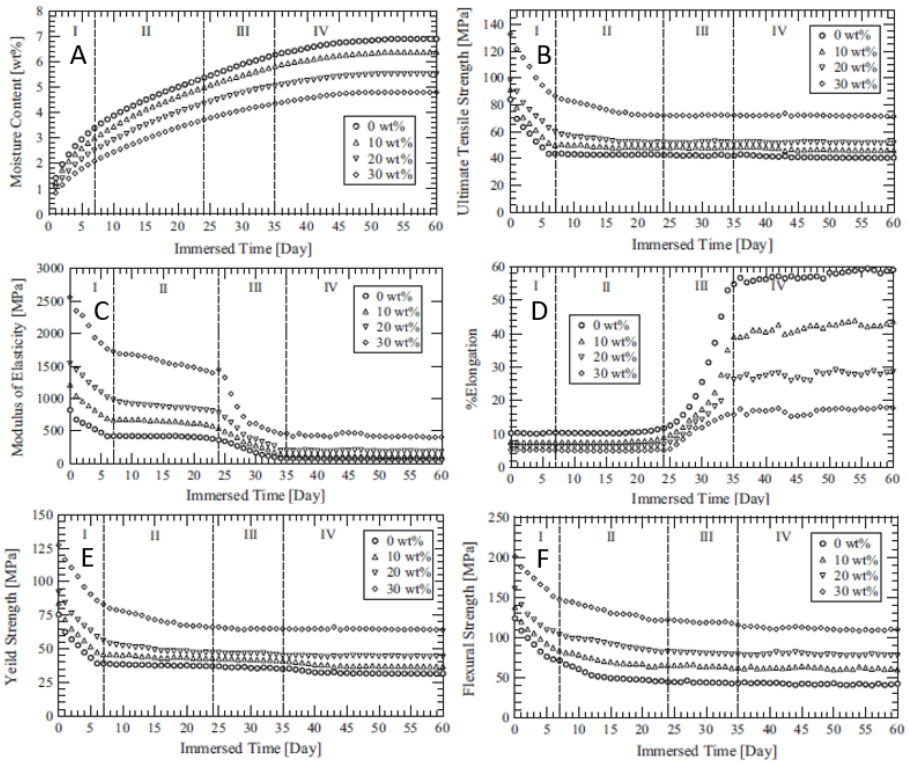

Figure 2.27: Experimental results of (A) moisture content, (B) ultimate tensile strength, (C) modulus of elasticity, (D) elongation, (E) yield strength, and (F) flexural strength versus immersed time in distilled water [13].

Pivdiablyk et. al. [14] had similar foundings in an experiment with PA 6. Specimens with various fibre directions (0°, 45°, and 90 °) where tensile tested in different temperatures after being exposed to 0 %, 50 %, and 85 % RH. The results show degradation in stress with increasing temperature and increasing RH, but increasing elongation.

2.5 Injection Molding of SFRP

Injection moulding is one of the most used production method considering thermoplastic polymers. It has large flexibility in design and it is a perfect solution for mass production due to the rapid processing and low cost at large production volumes [1]. Injection-moulded products can be found in various fields of use, even substituting metal parts. To reach a sufficient strength and stiffness for a structural application, short glass fibres are often added to the polymer blend [15]. A typical injection moulding machine with its main parts are shown in figure 2.28.

The injection moulding process can be described in four steps. In the first step, the polymer pellets in the hopper are transferred through the heated barrel by the screw which causes the polymer to melt. In the second step, the screw is pushed forward which increases the pressure so that the melt is injected into the mould cavity through the nozzle and the sprue. In the third step, the pressure is kept to permit packing and continue the melt flow as the melt solidifies and shrinks. After

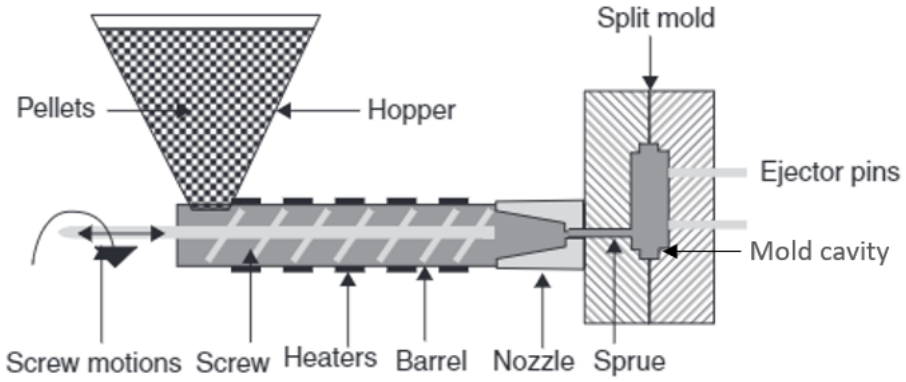

Figure 2.28: Illustration of the injection molding process [16].

sufficient cooling, the mould opens and the part is ejected using the ejector pin in the fourth and last step [17].

Using appropriate parameters in the process is crucial to avoid defects and obtain the wanted fibre orientation. Some of the factors that need to be considered are mould geometry, injection gate positions, injection speed, injection pressure, barrel temperature, mould temperature, mould thickness, holding pressure, notches, sharp corners, melt temperature and fibre content [15][18]. If these factors are considered together with the appropriate part design it is possible to avoid failures in the finished component.

For a SFRP, there are mainly two ways of manufacturing the pellet. The conventional way is to have the polymer matrix pellets and the short fibres in separate hoppers and mixed in a barrel before extrusion making the fibres randomly aligned into a short fibre pellet (SFP). The other method used is pultrusion where the matrix material is melted and infused into continuously unidirectional fibres in a long fibre pellet (LFP). Figure 2.29 illustrates the pellets from the two methods where the length of the pellets are typically 2-4 mm for the conventional method (a) and 10-12mm for the newer method (b) [16].

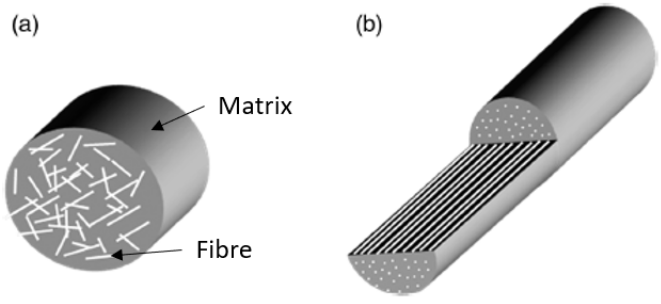

Figure 2.29: Illustration of (a) a SFP and (b) a LFP [16].

When the pellets are used in the injection moulding process, a severe fibre breakage may occur due to shear stresses caused by the injection screw. The fibre length reduction is around 10 % and 70 % for SFP and LFP respectively, causing a distinct reduction in fibre length distribution [17].

2.6 Defects in Injection Molding

Defects in the injection moulding process are quite common. Depending on the shape of the mould and other parameters such as mould temperature, injection speed, pressure, etc, these defects can largely be prevented. However, it is important to understand what the possible defects are, what causes them to occur, and what impacts they have on the properties of the part. Ten common defects in injection moulding are described.

2.6.1 Flow Lines

When the melt is injected into the mould it flows through the cavity until it is filled. The material is cooled continuously and eventually after the cavity is filled, it solidifies. Flow lines occur when the melt flows at varying speed causing the material to change direction, or leaves other visual structures. Others reasons to flow lines can be varying wall thickness or different solidifying speeds due to too low injection speed.

2.6.2 Weld Lines

Weld lines are formed when two flow fronts join, causing an inadequate bonding between the fronts. This defect often occurs when the mould is complex and contains multiple gates, inserts and thickness variations [19][20]. Weld lines are visible, hence they have a negative impact on the aesthetics of the part. But the most critical impacts is the lowering of mechanical properties due to three major factors: poor bonding adhesion, frozen-in parallel molecular orientation, and the existence of V-notches [21][22]. Often, weld lines can not be avoided, but having the intended design of the mould can place the weld line at a non-critical area concerning both structural and aesthetic demands [23].

Several investigations of what impact weld lines have on the mechanical properties have been performed. Zhou and Mallick [24] conducted a series of tensile tests with a polyamide (PA) polymer reinforced with 33 wt% short glass-fibre (PA33). The objective was to investigate the effect of fibre orientation and weld line formation on tensile properties. Another study where performed by Ozelik et. al. [25] who investigated the obstacle geometries and injection moulding parameters on weld line strength in tensile and impact test. The material used was plain polypropylene (PP). Demirer and Deniz [26], and Solymossy and Kovacs [27] both performed similar tests using PP30. A comparison of some mechanical properties from the previously mentioned tests is presented in table 2.2.

2.6.3 Vacuum voids

Vacuum void or sometimes called air entrapment are small pockets filled with air in the solidified material. There are two main reasons for these occurrences. The first one is due to that bubbles are formed from air, agents, degradation or contamination, and are brought into the mould. Usually, the moulding pressure is pushing the air

Table 2.2: Comparison of weld line impact on tensile strength from tests performed by Zhou and Mallick [24], Ozelik et. al. [25], Demirer and Deniz [26], and [27]

Article, material and test	E [min]	$\sigma_{F_{max}}$ [MPa]	ε_{ult} [MPa]
Zhou and Mallick			
PA33 parallel to MFD	7360	133.8	0.0393
PA33 normal to MFD	4430	86.51	0.0505
PA33 with WL	3800	67.53	0.03
Ozcelik et. al.			
PP without WL		22.1	0.47
PP with WL		19.7	0.05
Demerier and Deniz			
PP30 without WL		88.94	
PP30 with WL		41.97	
Solymossy and Kovacs			
PP30 without WL		38.3	
PP30 with WL		21.3	

out, but sometimes the air is trapped and causes the voids [28][20]. The other reason is too big differences in wall thickness. This can either cause some sections to solidify before the whole mould is filled, leaving unfilled voids, or raise the residual stresses, causing the part to cavitate, also leading to the formation of voids[1].

2.6.4 Surface Delamination

Surface delamination is a defect where the top layer of the part material is not sufficiently bonded to the underlying material which makes the surface flaky. This defect is caused by contamination or adding of incompatible materials causing failure in the bonds. Another reason for the defect could be excess of mold coating or moisture due to improper drying [20]. Also, the molecular orientation in the surface has a bi-axial orientation whereas the inner layer has more uniaxially aligned fibres [29].

2.6.5 Sink Marks

Sink marks are indentation on the surface of the part, usually where the part has a major change in thickness. These sink marks occur due to the contraction or shrinkage of the polymer melt during cooling. When the melt solidifies slowly the outer surface material is pulled inwards to create the sink mark. Some of the main reasons for the sink mars to occur are too slow solidification, too short and low holding pressure and time, and inappropriate thickness design [20][28].

2.6.6 Warping

Warping is when a part or sections of a part is bent or twisted after mould release and cooling. This is caused by residual stresses in the material induced by either

too quick cooling or to great differences in wall thicknesses [20].

2.6.7 Jetting

Jetting occurs when the injection rate is too high, causing an initial jet of melt into the mould cavity. When this jet touches the mould wall it starts to solidify before the whole cavity has been filled. This leaves a pattern of the jet on the part surface along with the decrease of mechanical properties due to insufficient bonding [20].

2.6.8 Flash

Flash is a protrusion of excess material at the edge of the moulded part. The most common places for this to occur is close to the gate or injector pin or at the line between two mould plates. The reason for it can be due to too high pressure, or that the mould is incorrectly designed or worn [20].

2.6.9 Short Shots

A short shot is what happens when the mould cavity is not completely filled by the melt. The main reason for this to occur is a design fault, where a section of the mould solidifies too fast. Either the material is too viscous, the section too narrow or the mould is too cold, which causes the material to solidify before the whole mould cavity is filled. Another reason can be the excess of air trapped in the mould cavity, preventing it to be filled.

2.7 Anisotropy in Short Glass Fibre Reinforced Thermoplastics

The term isotropy can be described as uniformity in all directions, often regarding mechanical properties. A homogeneous material like most metals and some polymers can be considered to be isotropic. However, when filler materials such as glass fibres are added, the material characteristics changes and generally accentuates anisotropy. The fibres in the polymer change properties of the material depending on the fibre direction causing the properties to differ in different directions [15]. Generally, the fibres would be aligned along the melt flow direction (MFD). But at further investigation, it can be seen that the material is reaching a skin-shell-core-shell-skin structure [15].

Through a computed tomography performed by Holstrom et. al. [15] the probability density function of the projected fibre angles was obtained for a Polyamide 6 (PA6) material with adding of 15 wt% (PA6 GF15) and 30 wt% (PA6 GF30) glass-fibre. Results indicate that the degree of fibre alignment in the MFD is high in the surface layers of the material, but decreases rapidly in the core layers [15]. For PA6 GF30, simulation of the skin-core-skin layers (a) and the fibre angle relative to the MFD (b) can be seen in figure 2.30.

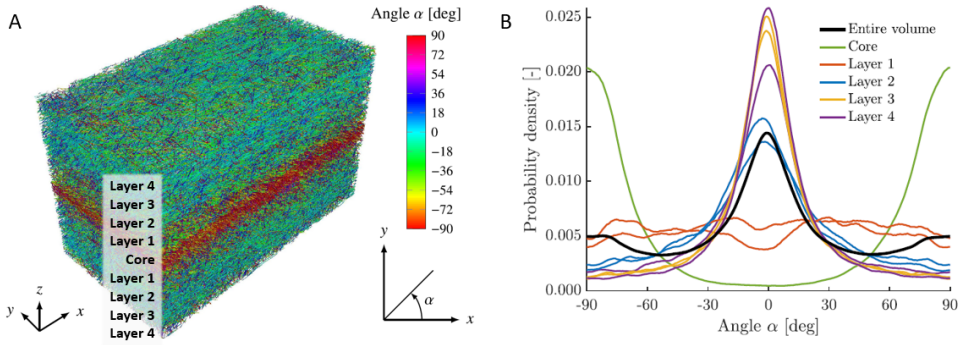

Figure 2.30: (a) Visual simulation of the skin-core-skin structure together with (b) probability density of the fibre angle (α) from MFD (x) [15].

Holmstrom et. al. [15] also performed a series of tensile tests to investigate the impact of fibre direction on strength, stiffness, fracture strain, and Poisson's ratio. The experiment included the two previously mentioned materials, PA6 GF15 and PA6 GF30, along with plain PA6. The general fibre direction was determined by the specimen orientation angle to the MFD. For PA6 GF15 and PA6 GF30, tests were performed with the orientation angle at 0°, 15°, 30°, 45°, 60°, 75°, and 90°. For PA6, a test was performed with the orientation angle at 0°, 45°, and 90°. Three tests were performed at each angle for all materials. A summary of the tensile tests is presented in table 2.3.

According to the result of Holmstrom et. al. [15], the unreinforced PA6 has an anisotropic material behaviour. This is explained by the fracture of the 0°-specimen before the material was cold drawn, which was not the case for the 45°- and 90°-specimens.

A gradual decrease of both Young's modulus and ultimate tensile strength can be seen in all material with increasing the specimen angle to the MFD. However, the maximum strain differs between the two fibre filled material. For PA6 GF15, the maximum strain increases during the first angle shifts and tend to stagnate after 60°. For PA6 GF30, a peak can be seen at 45°. This is presumed to be due to shear like deformation [15]. Furthermore, Holmstrom et. al. conclude that orthotropic elasticity is a reliable approximation for the investigated fibre-reinforced materials.

A similar tensile test was preformed by Mortazavian and Fatemi [30] who investigated anisotropy effect on tensile properties in combination with temperature changes. The material used in this test was a PA6 matrix with adding of 35 wt% glass-fibre and 10 wt% rubber. The orientation angle of the specimens in relation to the MFD in this tests where set to 0°, 45°, and 90°. Results from the tests at room temperature shows that the tensile strength and young's modulus relative to the 0°specimen experience a drop of about 33 % and 38 % for the 45°specimen and 33 % and 31 % for the 90°specimen respectively. The maximum strain was increased by 175 % for the 45°and 8 % for the 90°specimen.

Monte et. al. [31] also performed several tensile tests to investigate the anisotropic behaviour of glass-fibre reinforced PA66. The amount of added reinforcement material was 35 wt% and the specimen orientation angle to the MFD was set to 0°, 5°,

10°, 20°, 30°, 45°, 60°, and 90°. A summary of the tensile tests is presented in table 2.3.

Appelsved [32] has also investigated the anisotropic behaviour of glass-fibre reinforced PA6/66. This material was conditioned and reinforced with short glass fibre and tensile tested with specimens oriented at 0°, 30°, 60°, and 90°relative to the MFD. A summary of the tensile tests is presented in table 2.3.

Table 2.3: Comparison the impact of specimen angle relative to MFD on tensile properties from the tests performed by Holmstrom et. al. [15], Mortazavian and Fatemi [30], Monte et. al. [31], and Appelsved [32].

Material, article and specimen thickness	θ [deg]	E [MPa]	$\sigma_{F_{max}}$ [MPa]	ε_{ult} [-]	$\upsilon_{in-plane}$ [-]	$\upsilon_{out-of-plane}$ [-]
PA6 GF30	0	7319	136.2	0.059	0.41	0.39
Holmstrom	15	7006	130.2	0.070	0.41	0.45
3 mm	30	5902	116.7	0.094	0.42	0.41
	45	5122	103.1	0.145	0.41	0.42
	90	4967	98.3	0.069	0.23	0.53
PA6 GF35	0	7111	130	0.053		
Mortazavian	45	4444	87	0.147		
3 mm	90	4889	87	0.058		
PA66 GF35	0	8555	152	0.023		
Monte	10	8417	150			
3 mm	20	8056	147			
	30	7667	142			
	45	7167	132	0.033		
	90	7106	118	0.028		
PA6/66 GF	0	6000	107	0.051		
Appelsved	30	4125	84	0.068		
3 mm	60	2963	63	0.075		
	90	2486	60	0.088		

3

CAE - Predicting and Preventing in use Failure

An important step of the product development process is to verify that the developed component will withstand the loads when it is used which can be done through mechanical testing. However, doing tests on finished products is expensive both since the component often is tested to failure, but also because if the component fails too early, it has to be redesigned. This is not only expensive but also time-consuming. One way to minimize premature failure in mechanical testing of the finished part is to use Computer Aided Engineering (CAE) before the product is manufactured. Using computational software to design and test is a time-efficient and an economical way of developing a new product.

The general CAE process includes the design of a 3D CAD model with subsequent Finite Element Analysis (FEA) of the model to determine its structural function. Depending on the material used in the component, different material models are used to decribe the material behaviour. At Thule, there is an interest in considering the fibre direction and some process-induced weaknesses of fibre reinforced polymers in the CAE. To realise this a mould flow analysis has to be done and transferred to the FEA software. FEA, material models, and mould flow analysis are described in the following sections.

3.1 Finite Element Analysis - LS-DYNA

FEA is a simulation of a physical component or phenomena using a numerical problem-solving methodology based on the Finite Element Method (FEM). Through the use of a calculating FEA software, it is possible to analyze real-world problems, such as structural analysis, fluid flow, and heat transfer, all in a computer. This is done by breaking down the overall problem into smaller and simpler parts that are easier to solve. These are the finite elements. These small elements are connected through the generation of a mesh that covers the whole body of the problem. For all element in the mesh, a partial differential equation is solved and combined to get an overall result. Hence, a higher density of elements requires more computational power, but the result will usually be more precise.

There are two main types of structural FEA, quasi-static and dynamic. Quasi-

static problems neglect intertial forces whereas problems do. Within these types of FEA, it is possible to have linear or nonlinear problems. When the linear static analysis is used for a structural problem the relationship between the applied force and displacement behaves linearly. The stress remains within the elastic range of the material and the stiffness matrix is constant. This is expressed as the following equation.

$$[K]\{u\} = \{f\} \tag{3.1}$$

Where $[K]$ is the stiffness matrix, $\{u\}$ is the displacement vector and $\{f\}$ is the load vector. If the problem follows the dynamic rules, the corresponding equation is formulated as.

$$[M]\{u''(t)\} + [C]\{u'(t)\} + [K]\{u(t)\} = \{f(t)\} \tag{3.2}$$

The $[M]$ is the mass matrix, $[C]$ is the damping matrix, $\{u''(t)\}$, $\{u'(t)\}$, $\{u(t)\}$, and $\{f(t)\}$ is the time varying acceleration, velocity, displacement, and load vector respectively.

If the problem instead is non-linear, there are three attributes of the system that can behave nonlinear, namely geometry, material, and constraints and contacts. This can include changing boundary conditions, large deformations, and material which do not exhibit linearly elastic behaviour.

When a nonlinear dynamic FEM is used there are two approaches regarding the time incrementation during solving. In the implicit approach, a global equilibrium has to be established for each time increment, which means each increment has to converge. This makes it possible to have big time increments but this means that the computing time is high. On the contrary, the explicit approach does not have to converge each increment and instead assume global equilibrium exists. For each increment, the local finite elements variables are calculated before continuing with the next one. This calculates each increment very fast, but to maintain the equilibrium and accuracy of the solution, the increments have to be very small.

The software that Thule uses for their FEA is called LS-DYNA which has a diverse use within multiple areas in need of FEA. The code that LS-DYNA is built from origins from highly nonlinear, transient dynamic FEA using explicit time integration.

The elements in the mesh can take various shapes with different calculating properties depending on what is of interest for a certain simulation. The different elements are described by its element formulation (ELFORM in LS-DYNA). The three most used shapes for solid elements are tetrahedrons, pentahedrons and hexahedrons. Another thing to consider when selecting element is its properties, especially when it comes to integration points and rotational degrees of freedom, and with this, the subsequent CPU time. For this report, there is a specific interest in two element formulations, named ELFORM 4 and ELFORM 13. Both have the shape of a tetrahedron but the major difference is the number of integration points. ELFORM

13 only has one, whereas ELFORM 4 has five. Also, ELFORM 4 has six degrees of freedom per node (three translation and three rotational) whereas ELFORM 13 only has three (translation). This causes ELFORM 13 to be a bit less accurate, but ELFORM 4 to require more CPU time since it is scalable to the amount of integration points [33].

3.2 Material Models - LS-DYNA

For the FEA to work properly, not only the shape and boundary conditions need to be correct, but also the material needs to have the right properties and behave correctly. This is included through a material model that includes all the important material parameters and properties for the devoted material. To get the right response characteristics of the material, the included parameters must be carefully chosen.

Materials such as metals are relatively well documented regarding material properties which makes it relatively easy to. For more complex materials such as composites, all properties can not be defined by simple parameters. Therefore, there could be a need of using multiple material models. It could also include the need for physical testing to find the right characteristics and fit them towards a material model. Furthermore, it is also necessary to fit the material model with the right failure criteria and damage model.

As mentioned previously, the material models are built from numerous attributes and parameters. There are seven attributes a model can include, which are described as follows [34].

STRATE	- Strain-rate effects
FAIL	- Failure criteria
EOS	- Equation-of-State required for 3D solids and 2D continuum elements
THERMAL	- Thermal effects
ANISO	- Anisotropic/orthotropic
DAM	- Damage effects
TENS	- Tension handled differently than compression in some manner

Furthermore, the parameters included in each model varies a lot. For each model there is a card including several parameters to capture the material characteristics. The variables include common properties such as Density, Young's modulus, Yield stress, etc, but also more uncommon or complex properties such as Load Curves, Damping factor, etc. [34].

Failure criteria are described by mathematical expressions. The expression captures the essential behaviour of a material during failure. Some common mathematical failure criteria are Tsai-Wu (brittle fracture), Tsai-Hill (brittle fracture), von Mises (yielding), Tresca (yielding), Chang-Chang, Puck etc. [34].

In this thesis, three material models distributed by LS-DYNA are evaluated and discussed for further implementation. These material models are; Mat_24 (piece-

wise linear plasticity), Mat_157 (anisotropic elastic-plastic), and Mat_215 (4A micromech). The attributes of these material models are presented in table 3.1.
Table 3.1: Material model attributes of the three evaluated materials [34].

Material	STRATE	FAIL	EOS	THERMAL	ANISO	DAM	TENS
Mat_24	X	X					
Mat_157					X		
Mat_215	X	X			X	X	

The material models can be tailored to fit a material better trough the usage of a software called LS-OPT. This software can be linked to LS-DYNA to perform various kinds of optimizations. Material models can be calibrated in Ls-OPT through repeated simulations of tensile tests varying parameters until the simulations agree with the physical tests.

3.2.1 Mat_24

Mat_24 is one of the most used material models in LS-DYNA due to its long history, reliable characteristics and relatively short computing time. The model is built on elastoplastic properties including arbitrary stress as a function of strain, with the possible inclusion of strain rate dependency [34]. The plasticity follows the von Mises theory. The strain rate can be accounted for in three options. One way is to use the Cowper and Symonds model, which scales the yield stress with a factor where strain rate is included. A second more general way is to use the variable LCSR which input a load curve to scale the yield stress where the scale factor is defined. A third way of including strain rate dependency is to reference the function to a table using the variable LCSS [34]. This material model is commonly used for metals, or as a typical go-to material model when unsure about what else to use.

For an application with a composite material, as in this case a short fibre reinforced polymer, a more complex material model is required. The model has to capture some essential properties which differ from a homogeneous isotropic material. Also, the properties of a composite material are highly dependent on the manufacturing method, which will be discussed later. Two models which possess the possibility to capture the right material behaviours are the Mat_157 and the recently developed Mat_215 [35]. These two models follow different principles.

The material card for Mat_24 is presented in figure A.1. The parameters for Mat_24 are described in table A.1.

3.2.2 Mat_157

Mat_157, is a combination of two models, the anisotropic elastic model Mat_002 and the anisotropic plastic model Mat_103_P. This model captures the anisotropic characteristics of a material such as a fibre filled polymer with plasticity following Hill's yield criterion. It is also possible to define Tsai-Wu or Tsai-Hill criterion for a brittle orthotropic failure. The model has a hybrid approach including both a micro and macro mechanical approach [34].

The macro-approach works on the composite such as it follows a linear elastic orthotropic material behaviour presented in section 2.3.5 which includes 9 material properties. These include tensile modulus in 3 axes, shear modulus in three planes, and Poisson's ratios, all following a local fibre coordinate system. All material model parameters have to be determined through material testing before the model can be used [34][35].

The micro-mechanics approach works on each constituent of the composite and instead follow the Mori-Tanaka model and includes material properties of all constituents. This part is important in order to consider the local fibre orientations in the material and to compute the anisotropic material data.

The material card for Mat_157 with all the input parameters for a solid material is presented in figure A.2. The parameters for Mat_157 are described in table A.2.

3.2.3 Mat_215

To consider the local anisotropy and fibre orientation in a short fibre reinforced material further, Mat_215 has been developed by 4A. The model is based on the calculation of thermoplastic composite properties using the Mori-Tanaka (Mean Field) Theory, Eshelby's inclusion model and orientation averaging. The model also includes a elasto-viscoplastic matrix behaviour and fibre and matrix failure can be implemented through maximum stress criterion and damage initiation and evolution model (DIEM) respectively [35].

The material card for Mat_215 is presented in figure A.3. The parameters for Mat_215 are described in table A.3.

Further description of the material models for Mat_24, Mat_157, and Mat_215 and their parameters can be found in [34].

3.3 Mold Flow Analysis - moldex3D

To analyse the melt flow and fibre direction of an injection moulded component with fibre reinforcement, Thule uses Moldex3D [36]. Similarly to FEA, the CAD model of the component is imported and a finite element mesh with the proper parameters, size, and geometry is generated. Inlets to the mould are placed and the parameters of the simulation set.

From the analysis, it is possible to see the melt flow in the mould and determine where possible defects can occur. Through tailoring of the process parameters, certain defects can be avoided or minimized. Also, by knowing where it is a high risk of defects it is possible to reconsider the design of the component or take the defect into account when the component is brought to FEA.

Another important function of Moldex3D is the prediction of fibre orientation since it has a big impact on the performance of the component. In each element of the mesh, a fibre direction is obtained which make it possible to visualize material

anisotropy and regions where fibre orientation is of interest. The results from the simulation can then be exported to a FEA software through a mapping tool called Envyo [37]. It uses a micromechanical interface to capture the wanted material properties. Hence, defects, fibre orientation and anisotropy can be considered in the structural FEA of a component. Through this type of analysis, it is possible to identify any potential issue and fix them before production.

4

Tensile Test of PA6 GF30

To obtain material properties and characterize the anisotropic mechanical behaviour of the PA30 material to be used in the Mat_157 material model, a tensile test where performed on specimen extracted from an injection moulded plate at angles of 0 °, 15°, 30°, 45°, 65°, and 90°relative to the MFD. Three tests were performed at each angle. Mould fill simulations of the injection moulded plate performed in Moldex3D and a tensile test of the specimens were simulated in LS-DYNA. These simulations was performed at angles of 0°, 45°and 90°relative to the MFD with the three material models Mat_24, Mat_157, and Mat_215.

4.1 Mechanical Tensile Test

The tensile tests of PA6 GF30 were conducted at Thule in Hillerstorp.

4.1.1 Setup - Mechanical Tensile Test

The experimental setup for the tensile test included a test rig (Instron 2530 test machine with a 50 kN static load cell), specimen grips (Instron 2716), extensometer (Instron 2639), software (Bluehill 3 [38]), and test specimens. An experimental setup is shown in figure 4.1.

Figure 4.1: Experimental setup for tensile tests.

Specimens were extracted from an injection moulded PA6 GF30 plates with the geometry 120x105x2 mm using water jet cutting. Two specimens were extracted from each plate as close to the centre of the plate as possible. The specimen dimensions were obtained from ISO 527-2 1AB standard and scaled to fit the plates. A model of the specimen with its dimensions can be seen in figure 4.2.

Three specimens were tested for each angle and two specimens at the same angle were extracted from each plate. For the 90°specimens, the grip of the specimen was slightly shortened to fit the plate. Specimens were pulled at a rate of 50 mm/min.

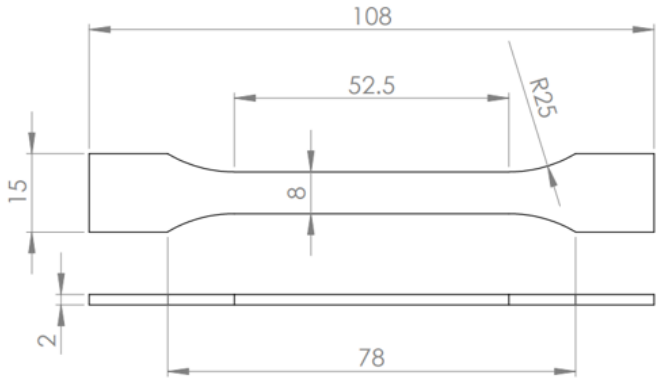

Figure 4.2: Dimension of tensile test specimens scaled from ISO 527 1AB.

The stress (σ) and strain (ε) was calculated according to the following equations.

$$\sigma = \frac{F}{A} = \frac{F}{w_0 t_0} \tag{4.1}$$

$$\varepsilon = \frac{l}{l_0} \tag{4.2}$$

Where w_0, t_0, and l_0 is the original width, thickness, and length respectively, F is the applied force, A is the cross-section area, and l is the final length.

4.1.2 Results - Mechanical Tensile Test

The stress-strain curves of tensile tests are plotted in figure 4.3.

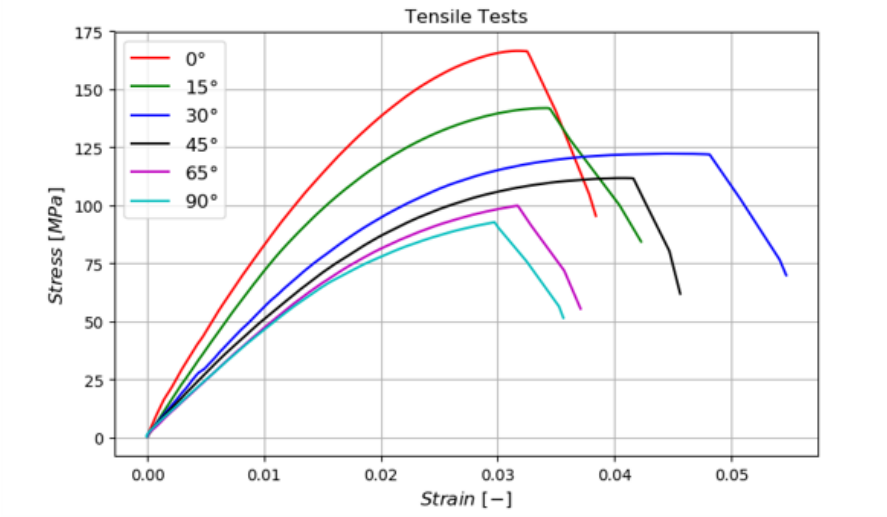

Figure 4.3: Stress strain curves from one tensile test per angle.

The mean value of Young's modulus and ultimate tensile strength and strain at fracture from all tests are presented in table 4.1.

Table 4.1: Test results from tensile tests of PA6 GF30 specimen at different angles.

θ [°]	E [MPa]	σF_{max} [MPa]	ε_{ult} [-]
0	8700	166	0.032
15	7800	142	0.034
30	6200	122	0.048
45	5400	111	0.042
65	4900	99	0.031
90	4600	93	0.030

The fracture of all specimens are presented in figure 4.4.

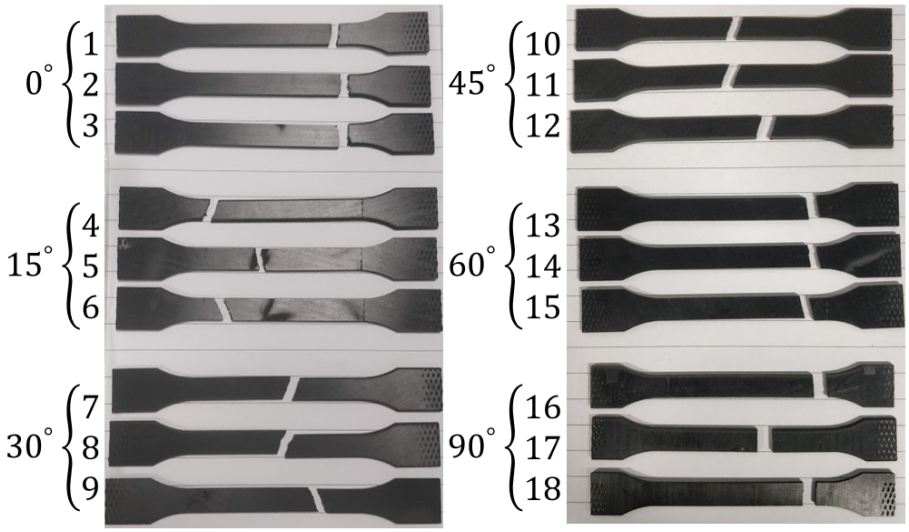

Figure 4.4: Fracture of all specimens at different angles.

4.2 Simulation of Tensile Test

The simulation of the tensile test of PA6 GF30 were carried out at Thule in Hillerstorp.

4.2.1 Setup - Simulation in Moldex3D

A CAD model of the injection moulded specimen plate was modelled and imported to Moldex3D. Inlet was placed along one short side of the plate. A mesh was generated with 1.5 mm element length and with the shape of a prism. The plate with the mesh and inlet can be seen in figure 4.5.

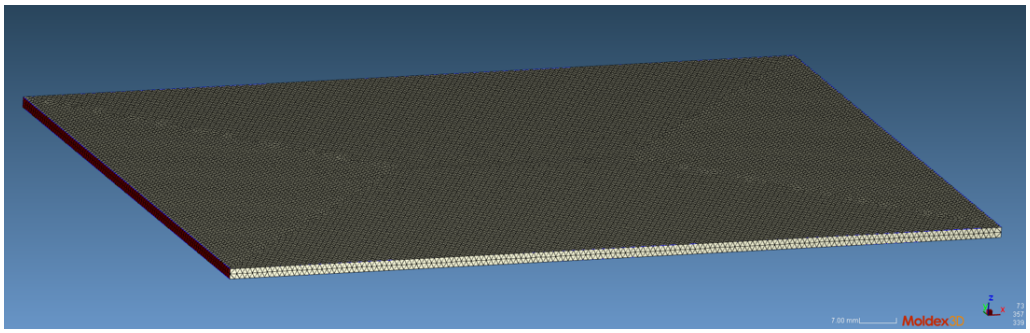

Figure 4.5: Plate in Moldex3D with finite element mesh and inlet marked in red.

Material Grilon BG30 was selected and process parameters were selected according to manufacturing recommendations.

4.2.2 Result - Simulation in Moldex3D

Degree of fibre orientation in the skin layer of the injection moulded plate can be seen in figure 4.6.

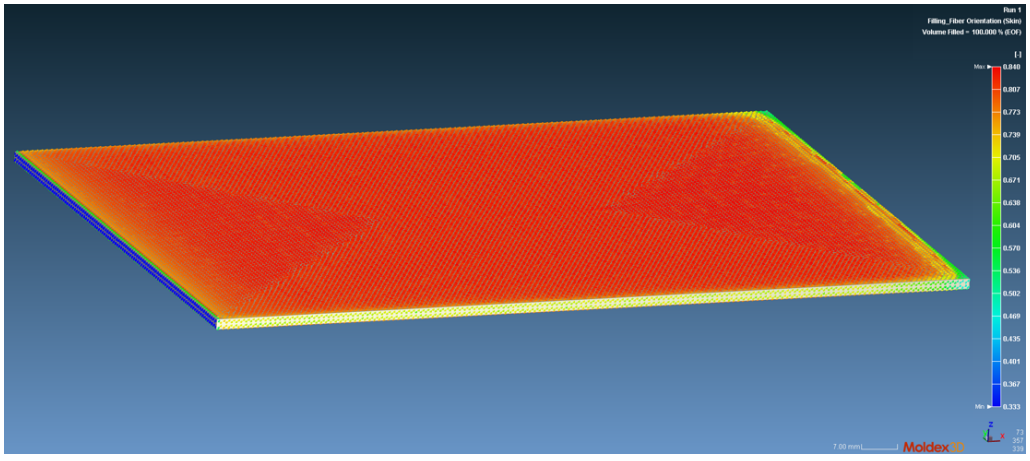

Figure 4.6: Degree of fibre orientation in the skin layer of the injection moulded plate. The colour scale denotes the degree of orientation; red denotes highly oriented fibres, whereas blue denotes randomly oriented fibres.

Degree of fibre orientations in cross-sections transverse and parallel to the MFD in the injection moulded plate can be seen in figure 4.7.

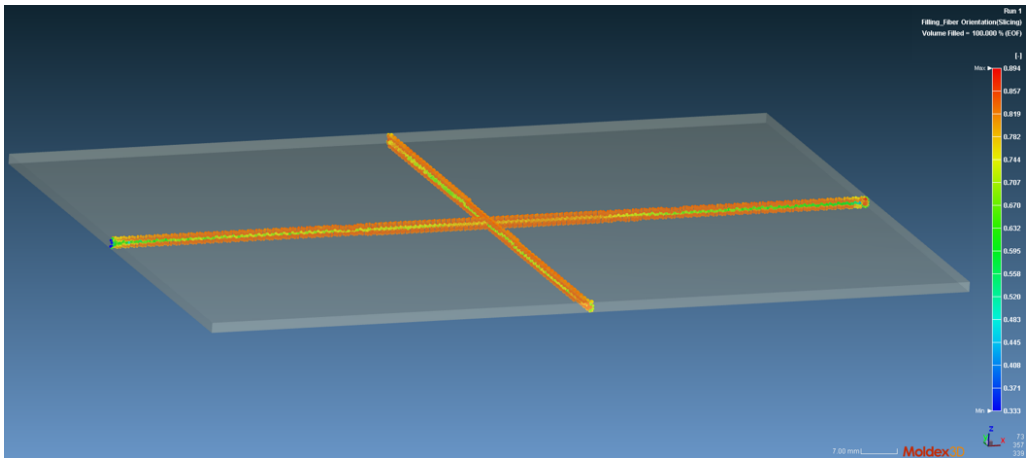

Figure 4.7: Degree of fibre orientation in the two cross-sections of the injection moulded plate. The colour scale denotes the degree of orientation; red denotes highly oriented fibres, whereas blue denotes randomly oriented fibres.

4.2.3 Setup - Simulation of Tensile Test

A tensile test specimen of the same dimension as the specimens in the mechanical testing was modelled and imported to LS-DYNA. A mesh with ELFORM 16 shells with five integration point through the thickness was generated. The local fibre direction and distribution obtained from the simulation in Moldex3D were mapped to the specimen model in LS-DYNA at 0°, 45°, and 90°using Envyo [37]. The grip on one side of the specimen (red cross) was assigned a fixed boundary condition and the other grip (red arrow) was displaced according to figure 4.8.

Figure 4.8: Setup of the tensile test simulation. The red cross indicates the fixed boundary condition and the red arrow indicates the displacement.

All simulations was performed in LS-DYNA using an explicit solver.

4.2.4 Results - Simulation of Tensile Test

The stress-strain curves from simulation of tensile test with 0°and 90°specimens with material model Mat_24, Mat_157, and Mat_215 are plotted in figure 4.9.

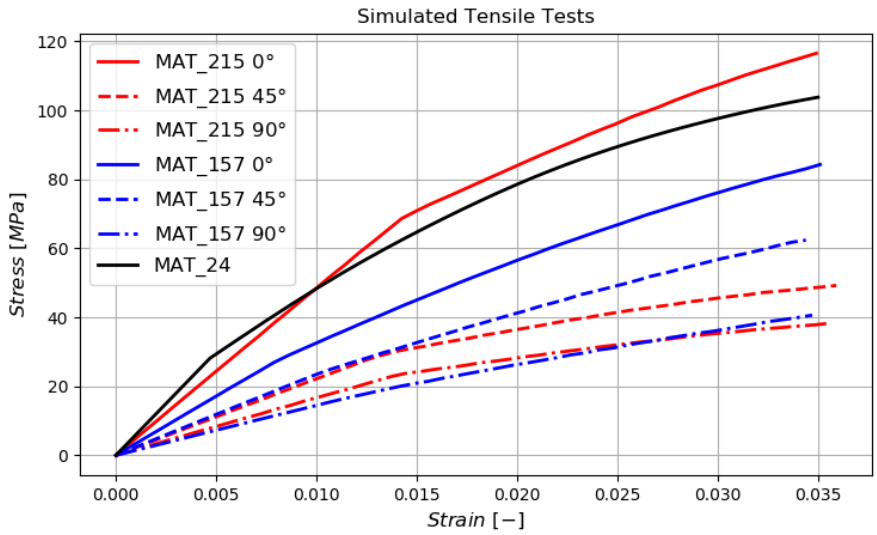

Figure 4.9: Stress-strain curves from simulation of tensile test of 0°and 90°specimens with material model Mat_24, Mat_157, Mat_215 and result from mechanical tensile test.

4.3 Discussion - Tensile Test of PA6 GF30

In accordance with the literature [5][15][6][30][14][31][32], the tensile test results in figure 4.3 and table 4.1 indicates that the fibre orientation in a material has a huge influence of the material properties. Highly oriented fibres in the direction of the load increase the strength significantly. It can also be seen in figure 4.3 and table 4.1 that the drop in strength decreases as the fibres are angled away from the direction of the load. The difference in strength between the 0°and 45°specimens is much higher than the difference between the 45°and 90°specimens. Also, the strain at fracture follows previous research indicating an increase in strain at fracture for the 30°and 45°specimens.

An effect of this can also be seen in the fractures of the specimens in figure 4.4, where the angle of the fractures differs. The 0°and 90°specimens fracture transverse to the load direction, whereas the other specimens in between have a tilted fracture surface. This could imply that the strength is more dependent on the shear stress.

If the results obtained from the tensile test in this project is compared to the literature [15][30][31][32] further, it is possible to distinguish a difference in the drop in strength from the 0°to the 90°tests. The strength is lowered with around 44 % in the test performed in this project whereas its lowered by 28 %[15], 33%[30], 22 %[31], and 44 %[32] for the test in the investigated literature. There are also significant differences in the stiffness drop; 47%, 32 %, 31 %, 17 %, and 59% respectively. The reason for these high differences can be due to several reasons. Young's modulus can be calculated in various manners and some of the values are obtained simply from analysing tensile test graphs which gives some error margin. Moreover, there are especially three physical reasons worth mentioning; material conditioning, specimen thickness, and constitutive materials. As previously mentioned the conditioning of

PA materials has a huge influence on the properties. The specimens in this project were not conditioned at all, and it is not clear in all the literature if and what conditioning was done. There is a high possibility that different conditioned materials give different changes in material strength and stiffness. Furthermore, the specimen thickness has some impact on the properties. As written by Fu [5], and confirmed in testing by [31], a thinner material will show bigger changes in strength and stiffness since the skin-core-skin phenomena are not as clear and the fibres are more aligned along the MFD. The specimens in this project had a thickness of 2 mm whereas literature mostly investigated a thickness of 3 mm. The last important factor is that both the matrix material and the glass fibre might have different properties. The matrix material used in literature is PA6, PA66, and combinations, which all have differences in properties. The properties can also be different within different types of PA materials, giving a big spread in material properties. Also, the added fibres can differ in both material properties and aspect ratio and length.

The tensile test specimens were as mentioned extracted from an injection moulded plate with the geometry 120x105x2 mm using water jet cutting. The reason for the scaled version of the ISO 527-2 standard size of the test specimen was to fit the extensometer on a 50 mm length with constant cross-section. The grip section of the 90°samples had to be shortened slightly due to the difference between the length of the specimen and the width of the plate. This could affect the results due to less grip strength.

Deviations in the result could also occur from the water jet cutting production method of the specimens. The method may introduce defects at the cutting surface which could lead to premature failure and lower the failure strain of the material. These defects could be minimized through grinding, but due to time constraints, this step was skipped. However, since there are no significant deviations between the three test at each angle, the impact of such defects can be neglected in these tests.

Something highly important to take into account is that the specimens had not been exposed to any conditioning environment. As discussed in theory the effect of moisture absorption in PA6 has a great impact on material properties. Therefore, caution should be taken when comparing the results from these tests with other articles.

The melt flow simulation in Moldex3D was simplified to the extent that the inlet was placed along the whole cross-section. This was done since the inlet place and size was not know and to get the fibres oriented properly in the whole plate to make the fibre mapping better. As seen in the resulting figures 4.6 and 4.7, the red and orange colour denotes that the fibres at the skin and shell layers are highly oriented along the MFD. The lighter green colour in the core of the plate shows that the fibres are less oriented. These results are well aligned with the skin-core-skin theory [5][15].

The results of the tensile test simulation in figure 4.9 indicates similarities to the mechanical tensile test. However, these results are not completely comparable to the

mechanical tensile test since the material used there was not conditioned, whereas the material selected in the simulations is. Nevertheless, the difference between the 0°and the 45°and 90°tests are much more significant in the simulated test compared to the mechanical test. The mould flow simulation may suppose a too high fibre alignment through the thickness causing the drop in strength for the 90°specimen too high. The drop in strength between 0°and 90°is only about 45 % for the mechanical tests, while it is about 57 % and 76 % for the simulations using mat_215 and mat_157 respectively.

Continuing with comparing only the results for the three material models, the most obvious difference between them is that mat_24 has the same strength at both 0°and 90°due to the nature of the material model being homogeneous and isotropic. The upside of using mat_215 or mat_157 is that the anisotropic behaviour of a glass fibre reinforced polymer can be captured. A more interesting difference in the result is that mat_24 has the stiffest behaviour, mat_215 the second, and mat_157 the least. Even though the differences are not big, and the fracture load is similar this can cause risks when used on a product. Mat_24 might suppose a too high stiffness (and strength) in some directions causing the component to be under dimensioned. There are safety factors implemented to minimize that risk, but by using mat_215 or mat_157 the dimensioning of a component can probably be optimized.

The idea of doing a simulation of the tensile test is to capture the same behaviour of the material in the simulation as in the physical testing. As discussed in the two previous paragraphs, the behaviour of the material models does not follow reality completely. Through the use of LS-OPT it will be possible to calibrate the material curves for the different direction by changing some of the input parameters. How this will be done for each material model is out of scope for this project but will be crucial for the functionality of the models in the future. Important to consider is that if the parameters in the material models are changed too much, material behaviour that is not visible in the tensile test may be changed. Hence, it is important to consider this.

5

Case Study - Thule OutWay Hanging Bike Rack

A case study was conducted to compare flow simulation in moldex3D and FEA in LS-Dyna with real component testing. The component is already available on the market, hence, it has passed all the structural requirements. It is used only for the investigation of the reliability of the simulation software.

5.1 The component - Thule OutWay Hanging Bike Rack

The investigated component is a structural and functional console on the Thule Outway Hanging Bike rack, a "rear door" hanging bike rack. The complete bike rack in use (a) and a magnification of the console (b) is shown in figure 5.1.

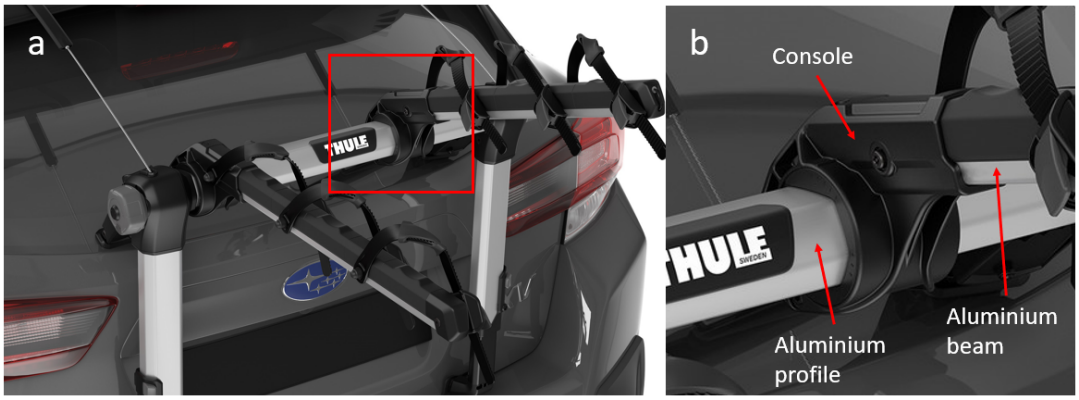

Figure 5.1: (a) Thule Outway Haning Bike Rack and (b) the investigated console with aluminium beam and profile.

Up to three bikes are loaded on the aluminium beams which are fastened in the console. The console transfers the load from the bikes into an aluminium profile which in turn transfer the load to the contact points to the car. The console can be turned around the profile and is fixed in place through a locking mechanism including teethes on the console and several groves in the profile.

5.2 Mechanical testing

To have a viable comparison to the simulations, four consoles with beam and profile were mechanically tested.

5.2.1 Setup - Mechanical Testing

The setup for the mechanical testing of the console included a test rig (ABUS D-5270 crane system and a table), load sensor (), extensometer (Sick BCG05-L1KM01PP), software (), and console specimens. A setup is shown in figure 5.2.

Figure 5.2: Experimental setup for mechanical testing of console.

This setup simulates a load applied at a point approximately 510 mm from the centre of the profile until failure. The load was applied at a constant rate of 20 mm/sek.

5.2.2 Result - Mechanical Testing

The load versus displacement curve from the mechanical testing of the four consoles is presented in figure 5.3. Two of the consoles (Test 2 and 3) did not fracture before the fracture occurred at the profile. The fracture of console 1 is presented in figure 5.4 a. Figure 5.4 b is a close up of the fracture on the left side in relation to a, c is a close up of the fracture in a, and d is the fracture on the opposite side of a. The fracture of console 4 is presented in figure 5.5 a, and a close up of the fracture in b.

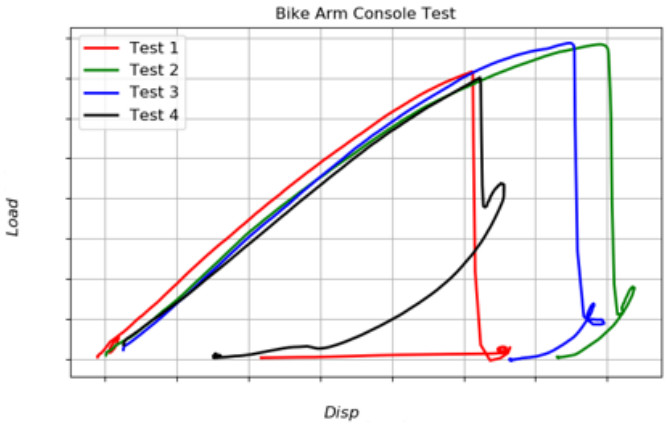

Figure 5.3: Load versus displacement curves for the mechanical testing of four consoles.

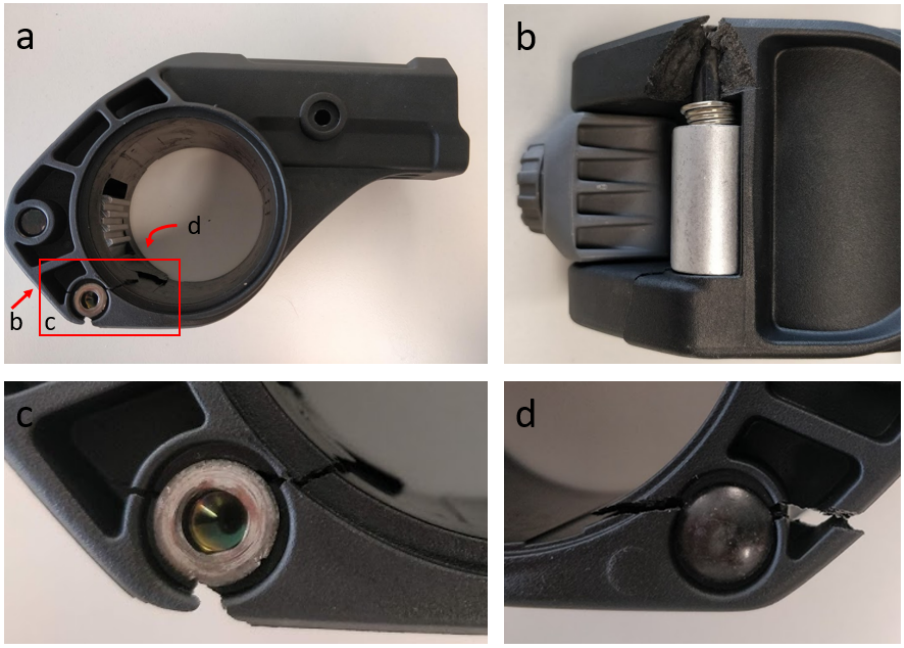

Figure 5.4: Fracture of console test 1 (a) and (b, c, d) close up of the fracture in at different directions.

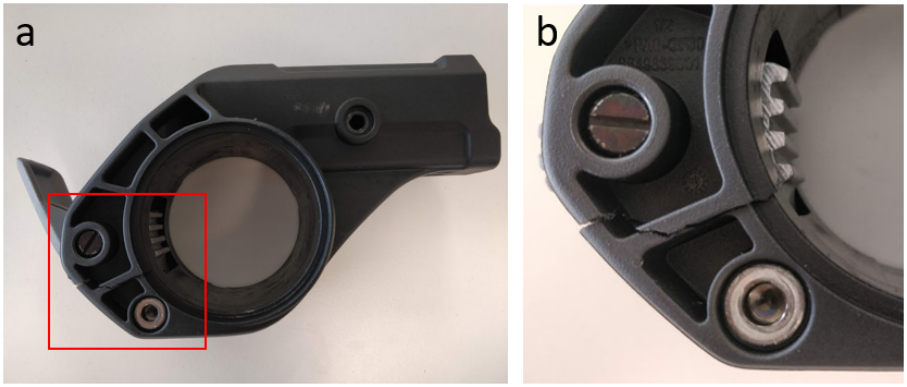

Figure 5.5: Fracture of console test 4 (a) and (b) close up of the fracture.

5.3 Simulation with Moldex3D

Moldex3D were used to perform a simulation of the melt flow in the moulding process of the console to capture the fibre direction and position of defects, especially weld lines.

5.3.1 Setup - Moldex3D

The CAD model of the console was imported to Moldex3D. Inlets were placed according to the visual imprints on the console. The inlet and the hot gate had a diameter of 2 and 5 mm respectively. A mesh was generated with various shapes of the elements, but with a base length of 1.5 mm. The console with the generated mesh and inlets is shown in figure 5.6 a and b.

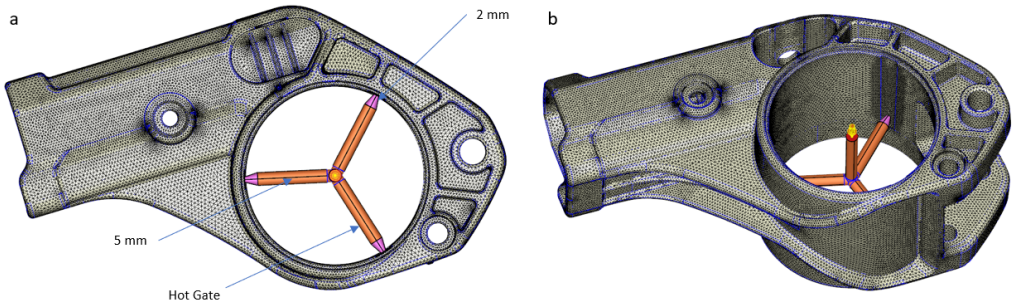

Figure 5.6: Setup of the simulation in Moldex3D visulised in (a) 2D and (b) 3D [36].

To capture the proper fibre characteristics and directions, since only one fibre direction is obtained for each element, the minimum number through the thickness is eleven. This results in prismatic elements as the first elements whereas the centre elements have a tetrahedral shape. A cross-section of the console is shown in figure 5.7 where the number of elements through the thickness and their shape can be seen. The total amount of elements was 1458518. Material Grilon BG30 were selected and process parameters were selected according to the manufacturing recommendations.

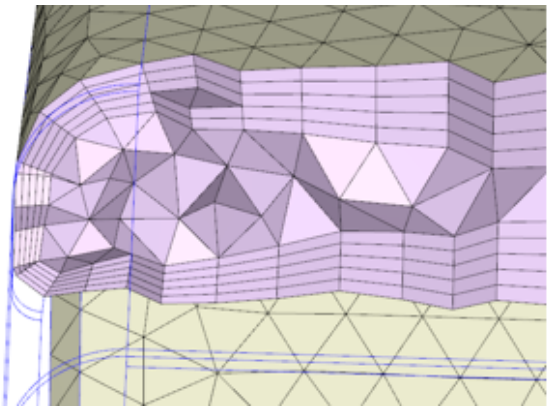

Figure 5.7: Cross section of the model to visualise element size in the thickness [36].

5.3.2 Results - Moldex3D

The simulated mould fill of the console can be seen in figure 5.8 (a-e) at 15% to 100% volume filled.

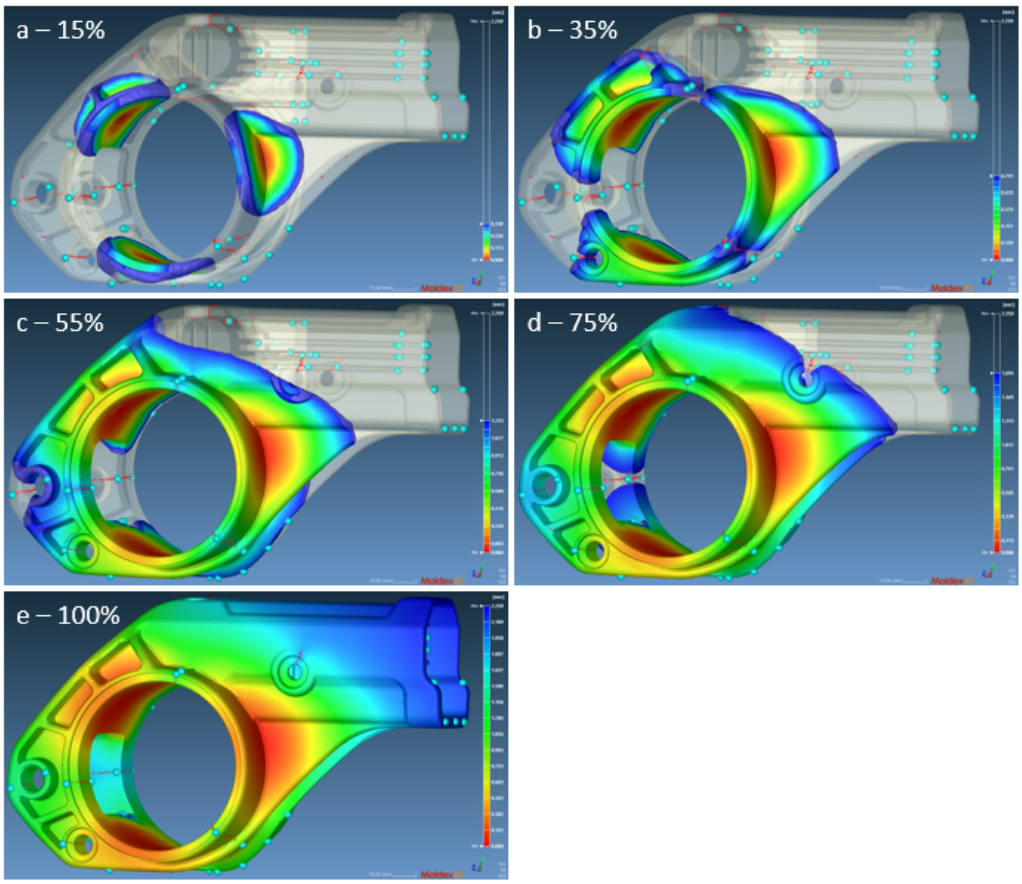

Figure 5.8: Simulated mould fill at (a) 15%, (b) 35%, (c) 55%, (d) 75%, and (e) 100% volume filled. The colour scale denotes the melt movement over time; blue denotes the most recent changes, whereas red denotes the first. The red lines and the blue spheres marks the arising weld lines and air traps respectively.

A zoom in of an air trap is shown in figure 5.9

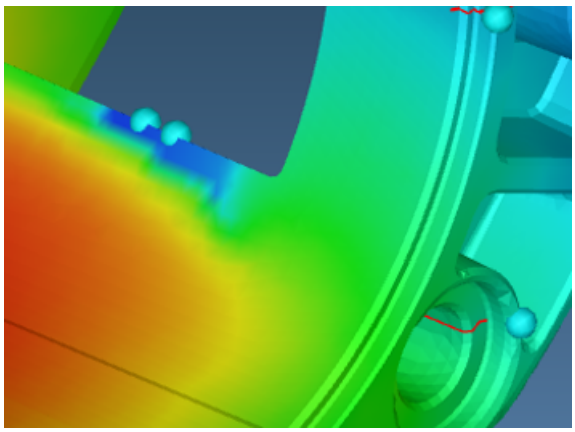

Figure 5.9: Zoom in of air trap. The blue spheres marks the arising air traps.

The simulated degree of fibre orientation in (a) the skin layer along with the fiber orientation in the (b) x-, (c) y-, and (d) z-direction is shown in figure 5.10.

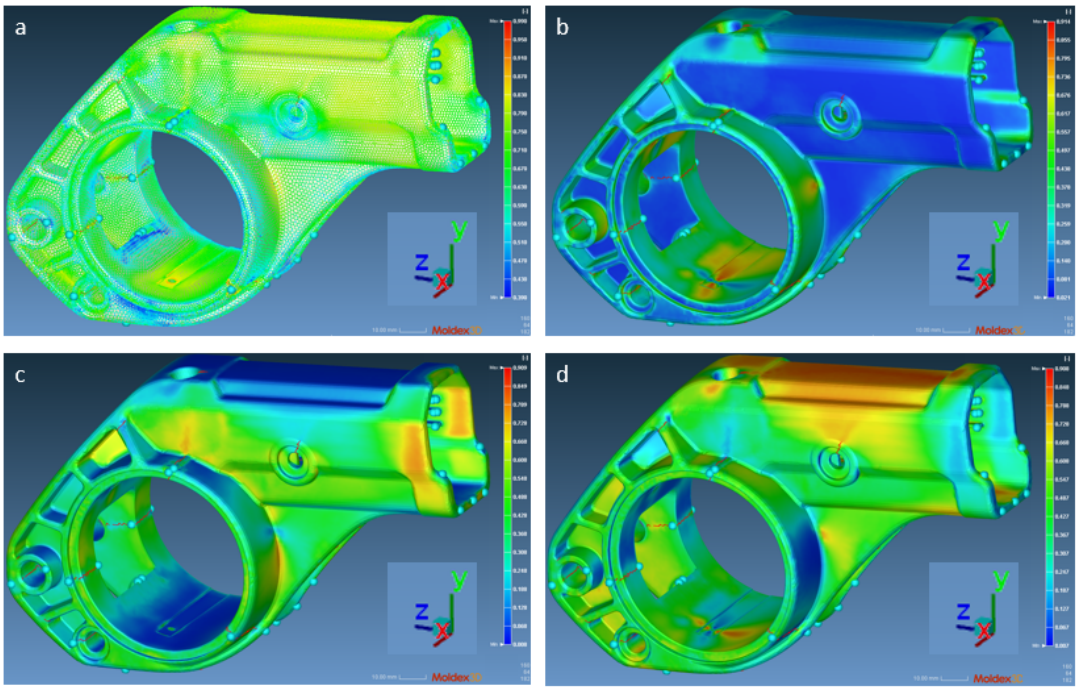

Figure 5.10: Simulated degree of fibre orientation in (a) the whole console and the amount of oriented fibres in the (b) x-, (c) y-, and (d) z-direction. The colour scale denotes the (a) degree of orientation and the (b, c, d) amount of fibres oriented in the respective direction. Red denotes (a) highly oriented fibres and (b, c, d) many oriented fibres, whereas blue denotes (a) randomly oriented fibres and (b, c, d) few oriented fibers.

A zoom in of the two lower holes from each side (a and b) is shown in figure 5.11. The degree of fibre orientation in a cross-section is displayed along with weld lines and air traps.

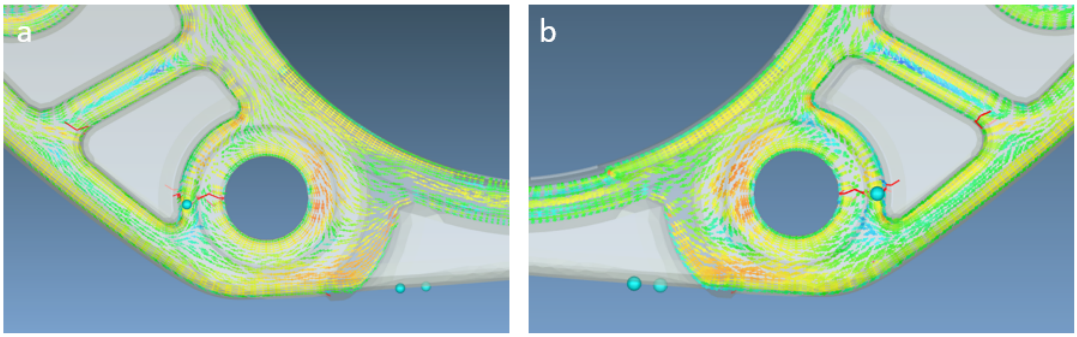

Figure 5.11: Degree of fibre orientation, weld lines and air traps at a cross-section of the lower wholes on each side.

5.4 Simulation with LS-DYNA

For the comparison to mechanical testing and the consideration of fibre direction and defects, the console was analysed in LS-DYNA with the three different material models (Mat_24, Mat_157, and Mat_215) described previously.

5.4.1 Setup - LS-DYNA

The CAD model of the console, together with the beam and profile were imported to LS-DYNA. A mesh was generated similar to the mesh in the flow analysis but using only ELFORM 4 with a length of 1.5 mm. The imported console (a) and the whole setup (b) is seen in figure 5.12.

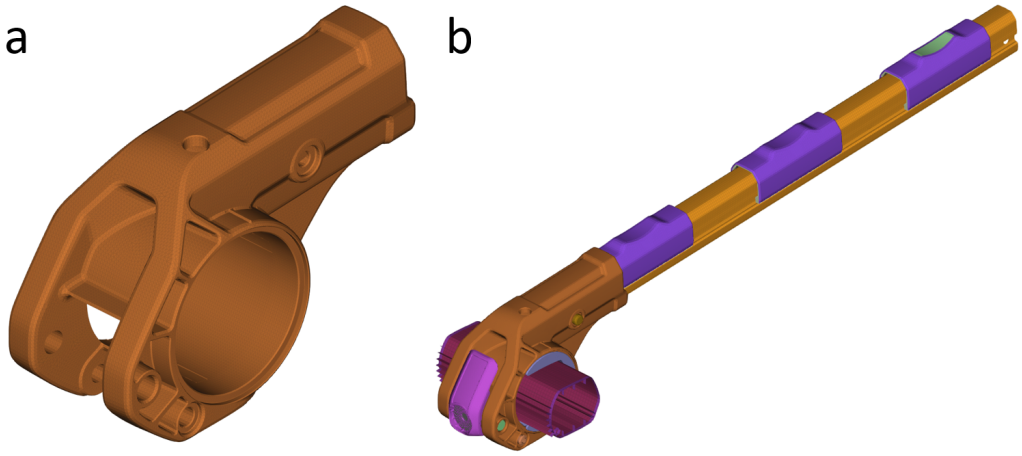

Figure 5.12: The imported console alone (a) and with beam and profile (b) for simulation in LS-DYNA.

The boundary condition of the edge of the profile was fixed as seen in figure 5.13 (a) and the load was applied on the beam 510 mm from the centre of the console as seen in figure 5.13 (b).

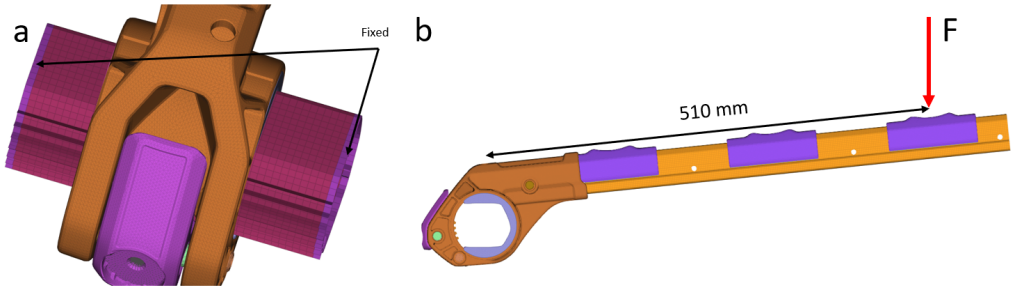

Figure 5.13: Boundary conditions (a) and applied load (b) for simulation in LS-DYNA.

The local fibre direction obtained from the simulation in Moldex3D were mapped to console model in LS-DYNA using Envyo [37]. A visual representation of the mapping is seen in figure 5.14.

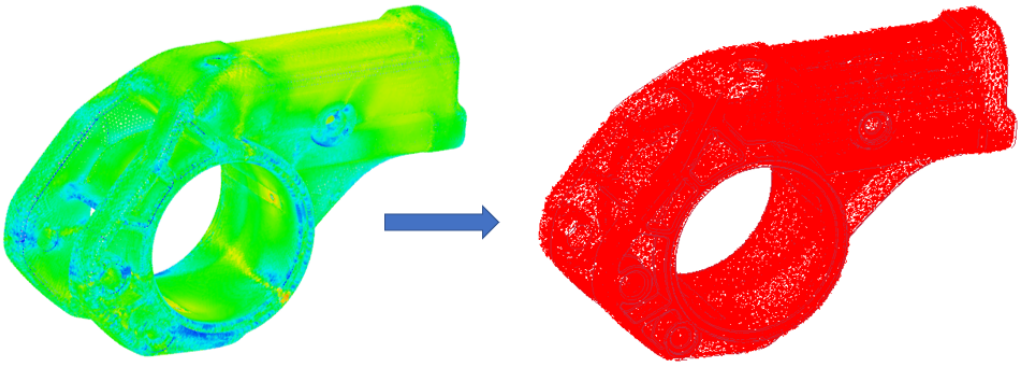

Figure 5.14: Visual representation of mapping fibre properties from moldex3D to LS-DYNA.

The material card used for simulation with Mat_24 is presented in figure B.1. The input parameters for the simulation was obtained from previously know material data and a stress-strain curve for PA6 GF30 seen in figure B.2.

The material card used for simulation with Mat_157 is presented in figure B.3. The input parameters are obtained from the mechanical tensile testing of PA6 GF30, the mapped fibre properties from Moldex3D and the material curve for PA6 GF30 seen in figure B.4. F, G, H, L, M, and N are the Hill's yield criterion constants calculated according to equations 2.30 to 2.35.

The material card used for simulation with Mat_215 is presented in figure B.5. Input parameters are obtained from material data of PA6 and the glass fibres used in production. The material curve for PA6 can be seen in figure B.6.

All simulations are run with an explicit solver and a static load. Parameters left at a value of 0 are set to a standard value determined by LS-DYNA.

5.4.2 Results - LS-DYNA

The load versus displacement curve from the mechanical testing of the four consoles along with the simulation using Mat_24, Mat_157, and Mat_215 is presented in figure 5.15.

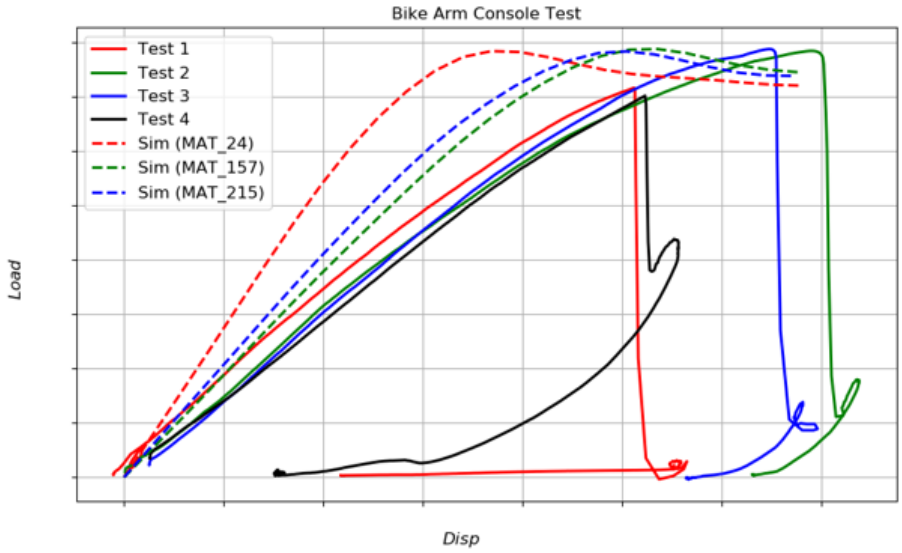

Figure 5.15: Load versus displacement curves for the mechanical testing of four consoles and simulations using Mat_24, Mat_157, and Mat_215.

To display and compare the results from the FEA, three points (P1, P2, P3) in the console where selected as seen in figure 3.1. P1 is is located at the circumference of the hole where fracture occurred in mechanical test 1, P2 at the locking mechanism, and P3 at the wall where the fracture occurred in mechanical test 4. Furthermore, a visual comparison of the simulation using material model Mat_157 (a) and Mat_215 can be seen in figure 5.16.

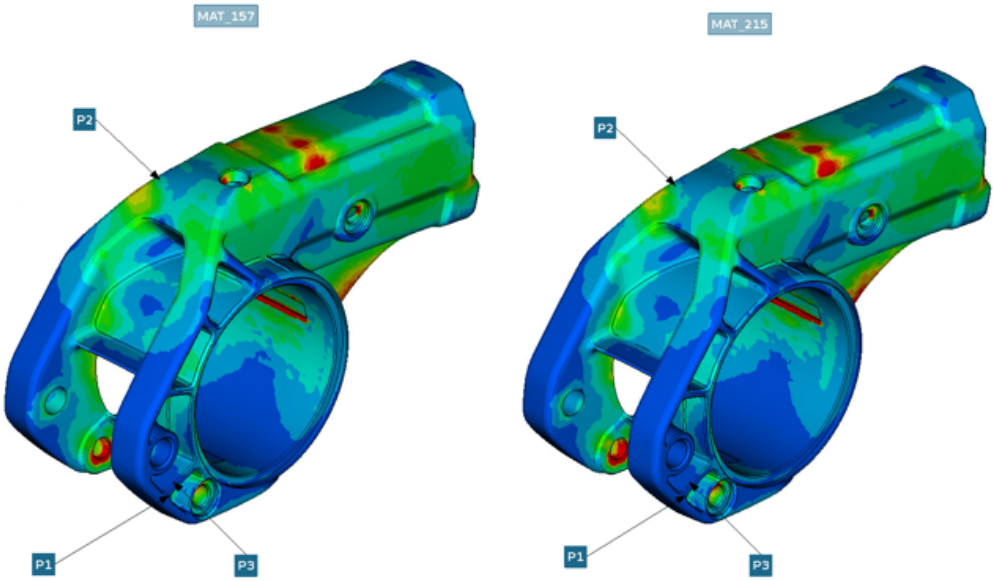

Figure 5.16: Visual comparison of FEA results using Mat_157 (a) and Mat_215 (b) including P1, P2, and P3. The colouring denotes the level of strain, where red is high strains and blue is low strains.

The von Mises stress-strain curves at the tree points can be seen in figure 5.17.

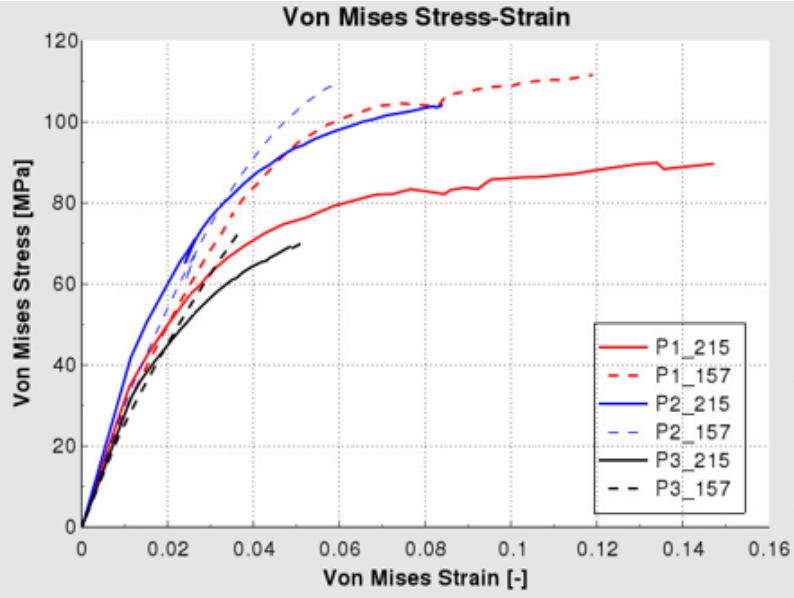

Figure 5.17: Von Mises stress-strain curve at P1, P2, and P3.

A zoom in on an (a) air trap and (b) P1 from a different angle are shown in figure 5.18.

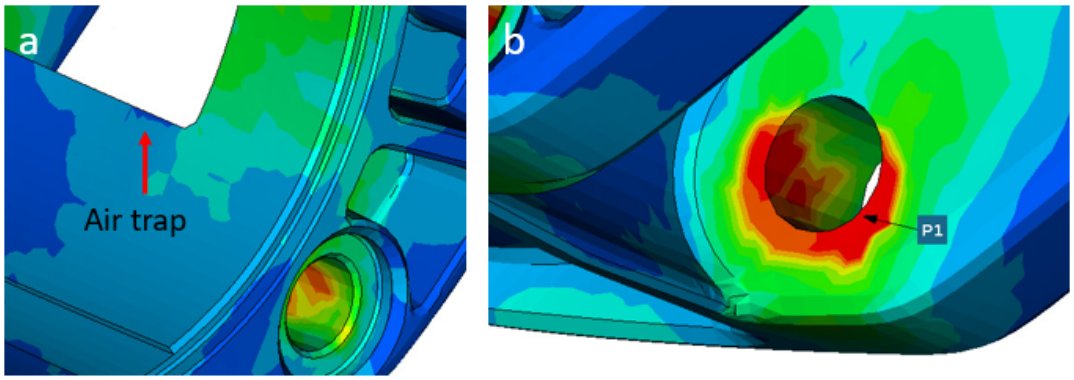

Figure 5.18: Zoom in on an (a) air trap and (b) P1 from a different angle. The colouring denotes the level of strain, where red is high strains and blue is low strains.

5.5 Discussion - Case Study

The resulting load-displacement curves from the mechanical tests of the components displayed in figure 5.3 along with the fractures of the consoles in figure 5.4 and 5.5 show how inconsistent a material can behave. Only two of the consoles (Test 1 and 4) fractured during testing. During the other two tests (Test 2 and 3), fractured occurred at the fastening mechanism at the profile when the load increased by about 10% compared to the fracture load for Test 1 and 4. As mentioned, this could be due to differences in the material of the console, since the injection moulding process is not always perfect and can induce defects as described in theory. Many of these defects are not possible to foresee and hard to discover from just looking at the fractures in figure 5.4 and 5.5. However, there is some correlation which can be seen

when bringing the melt flow analysis in Moldex3D into consideration, which will be discussed later. Another reason for the inconsistent results could have been due to defects or flaws induced from the previous usage of the consoles. Important to mention is that the console had been used for some kind of unknown testing before tested in this project. Even though there were no visual imprints, some minor defects could have been induced.

Figure 5.8 shows the simulated mould fill sequence of the console where the steps are selected to visualize important details and how weld lines and air traps occur. Since there are three inlets to the console and due to its design, weld lines are inevitable. The weld lines mainly occur around the smaller holes and when the melt front from each inlet meet. All weld lines are displayed in the figure by a thin red line and air traps are displayed as blue spheres. Figure 5.10 a, b, and c shows the amount of fibre oriented in x-, y-, and z-direction respectively and figure 5.10 d shows the degree of fibre orientation in all elements. Again, weld lines and air traps are displayed as red lines and blue spheres. By looking at these figures it is possible to see how the fibre orientation changes in the geometry and at the weld lines, especially at the skin layer where the stresses are the highest.

One defect that could have an impact on the performance is the air trap shown in figure 5.9. As seen in both figure 5.9 and 5.8 it can be seen that the place where the air trap occurs is filled with melt very late in the process due to the design of the component and the placement of the inlets. Through the use of mould fill analysis, it could have been detected and prevented through changes in either process parameters, component design or placing the inlets different. However, as seen in figure 5.18 a, the FEA shows that the strains in the area of the air trap are low and the fracture of the mechanical test did not occur in the area. If the air trap would be placed in a more critical place with higher stresses a mould fill and FEM analysis could prevent a defect like that to reach production.

A more significant defect for the result in this project is the weld line at the hole shown in figure 5.11 a. This is the same hole as in figure 5.4 c where the fracture of Test 1 occurred. Comparing the two figures, it is most likely that the upper left crack has occurred at the weld line. Similarly, for the hole on the opposite side of the console, the fracture shown in figure 5.4 d most likely occurred at the weld line in figure 5.11 b. Then the results from the FEA is considered. Figure 5.17, 5.18 b and 5.16 all includes P1 which is chosen at the location of the hole in figure 5.4 c. The red colour indicates a high local strain which is confirmed in figure 5.16. These high strains imply that fracture would occur in this region. Together with the result from the mould fill simulation, it is no coincidence that the fracture occurred here. Through the use of both mould fill simulation and FEA, a case like this can be considered early in the design process. It is not possible to remove the weld line, but it is possible to minimize its impact and increase the strength of the component.

Regarding the fracture of Test 4 in figure 5.5 a and b, it is harder to draw any conclusions. Comparing the fracture to both the mould fill simulation in figure 5.10 and 5.11, and the FEA in figure 5.16 and 5.17 it is hard to find any correlation. The FEA shows no indication of any high stress or strain and there are no indications of

any defects. In figure 5.11 there is a small indication that the fibres in the wall where the fracture occurred are a bit randomly aligned as the blue colour denotes. However, it feels unlikely that this would be the reason for the fracture. One possibility could be some inbuilt stress from production due to warping, but to draw a conclusion like that would require further analysis.

As mentioned, it is hard to distinguish which one of mat_215 and mat_157 that give the most reliable results. However, there is a huge advantage in using mat_215 since there is no particular need for time consuming material testing, which is the case for mat_157. Through the macro mechanics approach the matrix and reinforcement properties are inserted separately whereas parameters has to be calculated from results of tests in several directions. One downside found in mat_215 was that ELFROM 13 was not yet implemented in the solving which is the element formulation that Thule wishes to use due to its efficiency. Hence, ELFORM 4 had to be used instead. However, there are no fundamental problems with implementing ELFORM 13 so it will most likely be implemented in the future. In the contrary, it was not possible for mat_157 to be run with an implicit solver for an unknown reason.

The simulation using the three material models can be compared to the mechanical testing of the console in figure 5.15. All the material models show a stiffer behaviour than the actual testing. This could be due to that the models assume a too perfect material compared to the reality as discussed about the tensile test and that the input parameters of 30 % fibers and aspect ratio is not correct for the real material. Another reason for it could be deformations in the mechanical test that comes from the setup since the method was not verified to be completely reliable. More important is the analysis of the three points in figure 5.16 and 5.17 which shows three points of interest. If a mat_24 simulation would be included in the graph, it would display the same stress-strain relation for all points since mat_24 consider the stiffness to be the same in the whole material. This is not the case due to the fibre reinforcement, which can be captured by mat_215 and mat_157. Through the inclusion of the fibre orientation in the material models a greater understanding of the material behaviour in different places and geometries can be obtained. For example, the strain in P1 is very high. Hence, it would be motivated to assume that fracture would occur there, which it also did in mechanical Test 1. Regarding P2, the stress is relatively high, but the position of it is at a locking mechanism in metal which would probably hinder deformation. P3 shows as previously discussed, no tendency of high stresses and strains even though it fractured there. This confirms that materials does not always behave as expected and that further investigations are needed. The big difference in stress between mat_215 and mat_157 in P1 could be explained by the usage of input parameters obtained from tensile tests using unconditioned material. Nevertheless, it is still important to investigate which of the material model mat_215 and mat_157 that gives the most reliable results in simulation.

6

Conclusion

The results in this project show the benefits of implementing the combination of mould fill simulation together with FEA using adapted material models when developing new injection moulded components, especially using short glass fibre reinforced polymers as material. In the mould fill simulation, it is possible to bring awareness to the risk of defects in exposed areas. There is also the potential of getting an understanding of the anisotropic fibre orientation throughout the component and what impact different component design have on fibre orientation.

After the mould fill simulation, it is desirable to map the obtained result to the FEA software to implement the anisotropy and defects when structurally analysing the component through the usage of a material model created for fibre reinforced polymers. This enables the component to follow a more true behaviour compared to when using a material model which does not consider fibre orientation. Since the orientation of the fibres has shown to have a significant impact on both strength and stiffness, it is crucial to consider this to minimize the risk of failure after production and to optimize the material use and design. A summary of this sequence is described in table 6.1.

How well the function of capturing the anisotropic behaviour of a fibre reinforced material in Moldex3D works is hard to distinguish from the tests performed in this project. To gain full knowledge about that and how precise the weld line and air trap functions are, a more close analysis of the material would be needed. This would include microscopical analysis. However, it can be concluded that the mould fill simulation works to some degree and is a better choice than supposing isotropic and homogeneous material for the FEA.

The material models Mat_157 and Mat_215 used for fibre reinforced material in LS-DYNA are not yet fully developed and has not yet been implemented into the work at Thule. At the moment, the material models do not fully capture the right behaviour in all fibre direction. The material models probably suppose a to high degree of fibre orientation resulting in to stiff and strong material along the fibre, whereas transverse properties are to low. Hence, further testing of the material has to be done together with repeated simulations where the input parameters are tailored so that the material models are calibrated to the actual behaviour of the material.

Table 6.1: Description of the sequence when using simulation software.

STEP	**Description**
1. CAD	Import CAD of the investigated component to the mould fill simulation software (Moldex3D).
2. SETUP - MFS	Generate a suitable mesh for the component, select inlet placement and parameters, select material, and set processing parameters (Moldex3D).
3. SIMULATION - MFS	Run the simulation (Moldex3D).
4. ANALYSE - MFS	Analyse the result from the simulation to understand fibre anisotropy and possible defects (Moldex3D).
4. MAPPING	Map the fibre orientation to a FEA software (ENVYO).
6. SETUP - FEA	Generate a suitable mesh for the component. Set boundary conditions accordingly and place the load.
7. MATERIAL MODEL - FEA	Select a material model which has been calibrated to the material behaviour (LS-DYNA).
8. SIMULATION - FEA	Run the simulation with implicit or explicit solver (LS-DYNA).
9. ANALYSE - FEA	Analyse stress, strain and stiffness together with the analysis of the MFS to find areas with risk of premature failure. (LS-DYNA, Moldex3D)

7

Future Work and Recommendations

Since the tensile test in this project was performed using unconditioned PA6 GF30 a future tensile test using conditioned material is recommended. Both to see how the properties changes from unconditioned to conditioned, but also to get more realistic results to use in material models. With this comes the use of a software like LS-OPT to calibrate the material models to fit the material behaviour from the tensile tests.

Furthermore, investigations of implementing the weld line and air trap function from the simulation in Moldex3D in the FEA in LS-DYNA should be made. It is possible that these functions would bring further knowledge about weak parts in components but more analysis of both simulations and components are needed.

References

[1] N. G. McCrum, C. P. Buckley, and C. B. Bucknam, *Principles of Polymer Engineering (2nd Edition)*. Oxford University Press, 1997.

[2] D. Askeland and W. J. Wright, *The Science and Engineering of Materials*. Cengage Learning, 2016.

[3] G. H. B. Donato and M. Bianchi, "Pressure dependent yield criteria applied for improving design practices and integrity assessments against yielding of engineering polymers," *Jurnal of Materials Research and Technology*, vol. 1, pp. 2–7, 2012.

[4] A. N. Khan and B. A. Ahmed, "Comparative study of polyamide 6 reinforced with glass fibre and montmorillonite," *Polymer Bulletin*, vol. 72, pp. 1207–1216, 2015.

[5] S.-Y. Fu, B. Lauke, and Y.-W. Ma, *Science and engineering of short fibre reinforced polymer composite*. Woodhead Publishing Limite, 2013.

[6] K. K. Chawla, *Composite Materials: Science and engineering*. Springer, 2013.

[7] D. K. Rajak, D. D. Pagar, P. L. Menezes, and E. Linul, "Fiber-reinforced polymer composites: Manufacturing, properties, and applications," *Polymers*, vol. 11, 2014.

[8] B. Raju, S. Hiremath, and D. R. Mahapatra, "A review of micromechanics based models for effective elastic properties of reinforced polymer matrix composites," *Composite Structures*, vol. 204, pp. 607–619, 2018.

[9] D. Hull and T. Clyne, *An Introduction to Composite Materials*, 2nd ed. Cambridge University Press, 1996.

[10] R. F. Gibson, *Principle of Composite Materials*. McGraw-Hill, Inc., 1994.

[11] L. V. Pastukhov, M. J. W. Kanters, T. A. P. Engels, and L. E. Govaert, "Influence of fiber orientation, temperature and relative humidity on the long-term performance of short glass fiber reinforced polyamide 6," *Journal of Applied Polymer Science*, vol. 138, 2020.

[12] M. Kutz, *Applied Plastics Engineering Handbook: Processing, Materials, and Application*. Elsevier Inc., 2017.

[13] J. Chaichanawong, C. Thongchuea, and S. Areerat, "Effect of moisture on the mechanical properties of glass fiber reinforced polyamide composites," *Advanced Powder Technology*, vol. 27, pp. 898–902, 2016.

[14] I. Pivdiablyk, P. Rozycka, F. Jacquemin, L. Gornet, and S. Auger, "Experimental analysis of mechanical performance of glass fibre reinforced polyamide

6 under varying environmental conditions," *Composite Structures*, vol. 245, 2020.

[15] P. E. Holmström, O. S. Hopperstad, and A. H. Clausen, "Anisotropic tensile behaviour of short glass-fibre reinforced polyamide-6," *Composites*, vol. 2, 2020.

[16] A. Hodzic and R. Shanks, *Natural fibre composites: Materials, processes and properties*. Woodhead Publishing Limite, 2014.

[17] B. Parveen, "Fibre orientation and breakage in glass fibre reinforced polymer composite systems: Experimental validation of models for injection mouldings," 2015.

[18] A. A. Dzulkiplia and M. Azuddina, "Study of the effects of injection molding parameter on weld line formation," *Procedia Eng*, vol. 184, pp. 663–672, 2017.

[19] R. Zheng, R. I. Tanner, and X. J. Fan, *Injection Molding - Integration of Theory and Modeling Methods*. Springer, 2011.

[20] J. R. L. Valero, *Plastics Injection Molding - Scientific Molding, Recommendations, and Best Practices*. Hanser Publishers, 2020.

[21] H. Hagerman, "Weld-line fracture in molded parts," *Plast Eng*, vol. 29(10), pp. 67–69, 1973.

[22] T. Nguyen-Chung, "Flow analysis of the weld line formation during injection mold filling of thermoplastics," *Eng Comput*, vol. 43, pp. 240–245, 2004.

[23] M. Zhai, Y. Lam, and C. Au, "Runner sizing and weld line positioning for plastics injection molding with multiple gates," *Eng Comput*, vol. 21, pp. 218–224, 2006.

[24] Y. Zhou and P. K. Mallick, "A non-linear damage model for the tensile behavior of an injection molded short e-glass fiber reinforced polyamide-66," *Materials Science and Engineering*, vol. 393, pp. 303–309, 2004.

[25] B. Ozcelik, E. Kuram, and M. M. Topal, "Investigation the effects of obstacle geometries and injection molding parameters on weld line strength using experimental and finite element methods in plastic injection molding," *International Communications in Heat and Mass Transfer*, vol. 39, pp. 275–281, 2012.

[26] A. Demirer and S. Deniz, "Investigation of the effects of weld lines on the mechanical properties and energy consumption for injection moulded thermoplastics," *Energy Education Science and Technology*, vol. 29, pp. 1055–1062, 2012.

[27] B. Solymossy and J. G. Kovacs, "The examination of weld line properties in injection molded pp composites," *Materials Science Forum*, vol. 589, pp. 263–267, 2008.

[28] D. V. Rosato, D. V. Rosato, and M. G. Rosato, *Injection Molding Handbook*. Springer, 2000.

[29] Z. Tadmor and C. G. Gogos, *Principles of Polymer Processing*. John Wiley & Sons, 2006.

[30] S. Mortazavian and A. Fatemi, "Effects of fiber orientation and anisotropy on tensile strength and elastic modulus of short fiber reinforced polymer composites," *Composites*, vol. 72, pp. 116–129, 2015.

[31] M. D. Monte, E. Moosbrugger, and M. Quaresimin, "Influence of temperature and thickness on the off-axis behaviour of short glass fibre reinforced polyamide 6.6 – quasi-static loading," *Composites*, vol. 41, pp. 859–871, 2010.
[32] P. Appelsved, *Investigation of mechanical properties of thermoplastics with implementations of ls-dyna material models*, 2012.
[33] E. Tobias, *Review of solid element fomulations in ls-dyna*, 2011.
[34] LSTC, "Ls-dyna - keyword user's manual - volume ll material models," vol. 13582, 2021.
[35] P. Reithofer, A. Fertschej, B. Hirschmann, B. Jilka, A. Erhart, and S. Hartmann, "*mat_4a_micromech - theory and application notes," *International LS-DYNA Users Conference*, vol. 15, 2018.
[36] L. CoreTech System Co., *Moldex3d*, 2021.
[37] D. GmbH, *Envyo*, 2021.
[38] I. T. W. Inc., *Bluehill 3*, version 3.71, 2015.

A

Appendix 1 - Theory of Material Models

MAT_24 Material Card		MAT_PIECEWISE_LINEAR_PLASTICITY							
Notes	**Card**	**Parameters**							
	1	MID	RO	E	PR	SIGY	ETAN	FAIL	TDEL
	2	C	P	LCSS	LCR	VP			
	3	EPS1	EPS2	EPS3	EPS4	EPS5	EPS6	EPS7	EPS8
	4	ES1	ES2	ES3	ES4	ES5	ES6	ES7	ES8

Figure A.1: Material card with parameters for Mat_24 [34].

Table A.1: Definition of parameters in Mat_24 material card [34].

Parameters	**Description**
MID	Material identification.
RO	Mass density
PR	Poisson's ratio.
SIGY	Yield stress.
ETAN	Tangent modulus.
FAIL	Failure flag.
TDEL	Minimum time step size for automatic element deletion.
C	Strain rate parameter, C.
P	Strain rate parameter, p.
LCSS	Load cure ID or Table ID. Load Curve defines the effective stress as a function of effective plastic strain.
LCSR	Load curve ID defining strain rate scaling effect on yield stress.
VP	Formulation for rate effects.
EPS1 - EPS8	Effective plastic strain values.
ES1 - ES8	Corresponding yield stress values to EPS1 - EPS8.

MAT_157 Material Card		MAT_ANISOTROPIC_ELASTIC_PLASTIC							
Notes	**Card**	**Parameters**							
	1	MID	RO	SIGY	LCSS	QR1	CR1	QR2	CR2
	2	C11	C12	C13	C14	C15	C16	C22	C23
	3	C24	C25	C26	C33	C34	C35	C36	C44
For Solids	4b	C45	C46	C55	C56	C66	F	G	H
	5b	L	M	N		AOPT	VP		MACF
	6	XP	YP	ZP	A1	A2	A3		EXTRA
	7	V1	V2	V3	D1	D2	D3	BETA	IHIS

Figure A.2: Material card with variables for Mat_157 [34].

Table A.2: Definition of variables in Mat_157 material card [34].

Parameters	Description
LCSS	Load cure ID or Table ID. Load Curve defines the effective stress as a function of effective plastic strain.
QR1,2	Isotropic hardening parameter
CR1,2	Isotropic hardening parameter
C_{ij}	The ij^{th} term in the 6x6 anisotropic constitutive matrix.
F,G,H,L,M,N	Constants for Hill's yield criterion obtained from testing.
AOPT	Material axes options.
VP	Formulation for rate effect.
MACF	Material axes change flag.
XP,YP,ZP	Coordinates of point p for AOPT = 1and 4.
A1,A2,A3	Components of vector a for AOPT = 2.
Extra	Flag to input further data.
V1,V2,V3	Components of vector v for AOPT = 3 and 4
D1,D2,D3	Components of vector d for AOPT = 2
Beta	Material angle in degrees for AOPT = 0.
IHIS	Flag for material properties initialization. Allows mapping of local anisotropic data.

MAT_215 Material Card		MAT_4A_MICROMEC							
Notes	**Card**	**Parameters**							
	1	MID	MMOPT	BUPD			FAILM	FAILF	NUMINT
Fibre Orientation	2	AOPT	MACF	XP	YP	ZP	A1	A2	
	3	V1	V2	V3	D1	D2	D3	BETA	
Fibre Parameters	4	RVF		FL	FD		A11	A22	
	5	ROF	EL	ET	GLT	PRTL	PRTT		
	6	XT						SLIMXT	NCYRED
Matrix Parameters	7	ROM	E	PR					
	8	SIGYT	ETANT			EPSO	C		
	9	LCIDT				LCDI	UPF		

Figure A.3: Material card with variables for Mat_215 [34].

Table A.3: Definition of parameters in Mat_215 material card [34].

Parameters	**Description**
MID	Material identification.
MMOPT	Option to define elastic or elastic-plastic micromechanical material behaviour.
BUPD	Tolerance for update of strain-concentration tensor.
FAILM	Option for matrix failure - ductile DIEM-model.
FAILF	Option for fibre failure.
NUMINT	Number of failed integration points prior to element deletion.
FVF	Fibre-Volume-Fraction or Fibre-Mass-Fraction
FL	Fibre length. If FD = 1 then FL = aspect ration.
FD	Fibre diameter.
A11	Value of first principal fiber orientation.
A22	Value of second principal fiber orientation.
ROF	Mass density of fibre.
EL	E_L, Young's modulus of fibre - longitudinal direction.
ET	E_T, Young's modulus of fibre - transverse direction.
GLT	G_TL, Shear modulus LT.
PRTL	v_TL, Poisson's ratio TL.
PRTT	v_TT, Poisson's ratio TT.
XT	Fibre tensile strength - Longitudinal direction.
SLIMXT	Factor to determine the minimum stress limit in the fiber after stress maximum (fiber tension).
NCYRED	Number of cycles for stress reduction from maximum to minimum (fiber tension).
ROM	Mass density of matrix.
E	Young's modulus of matrix.
PR	Poisson's ratio of matrix.
SIGYT	Yield stress of matrix in tension
ETANT	Tangent modulus of matrix in tension.
EPS0	Quasi-static threshold strain rate (Johnson-Cook model) for bilinear hardening.
C	Johnson-Cook constant for bi-linear hardening.
LCIDT	Load curve ID or Table ID for defining effective stress versus effective plastic strain in tension of matrix material.
LCDI	Damage initiation parameter.

B

Appendix 2 - Material Models in Simulations

```
*MAT_PIECEWISE_LINEAR_PLASTICITY
$      MID        RO         E        PR      SIGY      ETAN      FAIL      TDEL
   2024001   1.35E-9      6000      0.35         0         0         0         0
$        C         P      LCSS      LCSR        VP       LCF
         0         0 202400101         0         0         0
$     EPS1      EPS2      EPS3      EPS4      EPS5      EPS6      EPS7      EPS8
         0         0         0         0         0         0         0         0
$      ES1       ES2       ES3       ES4       ES5       ES6       ES7       ES8
         0         0         0         0         0         0         0         0
```

Figure B.1: Mat_24 material card.

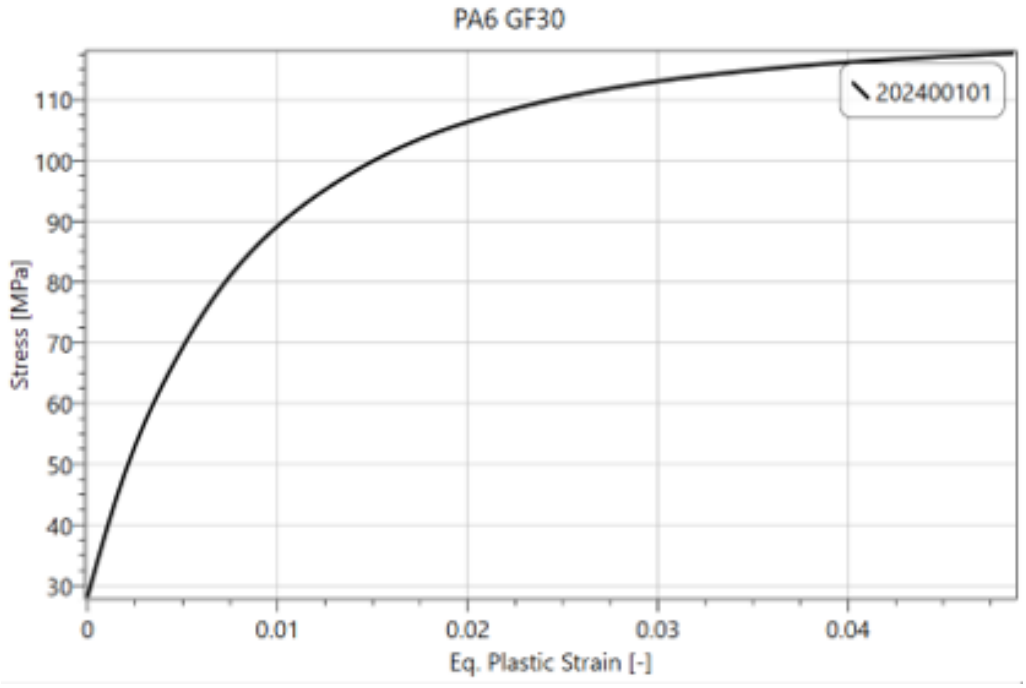

Figure B.2: Mat_24 material curve for PA6 GF30.

```
*MAT_ANISOTROPIC_ELASTIC_PLASTIC
$      MID        RO      SIGY      LCSS       QR1       CR1       QR2       CR2
  20157001    1.3e-9           02015700101         0         0         0         0
$      C11       C12       C13       C14       C15       C16       C22       C23
         0         0         0         0         0         0         0         0
$      C24       C25       C26       C33       C34       C35       C36       C44
         0         0         0         0         0         0         0         0
$      C45       C46       C55       C56       C66         F         G         H
         0         0         0         0         0       2.8       0.5       0.5
$        L         M         N                AOPT        VP                 MACF
       1.5       1.5       1.5                   0         0                    0
$       XP        YP        ZP        A1        A2        A3                 EXTRA
         0         0         0         0         0         0                    0
$       V1        V2        V3        D1        D2        D3      BETA      IHIS
         0         0         0         0         0         0         0         3
```

Figure B.3: Mat_157 material card.

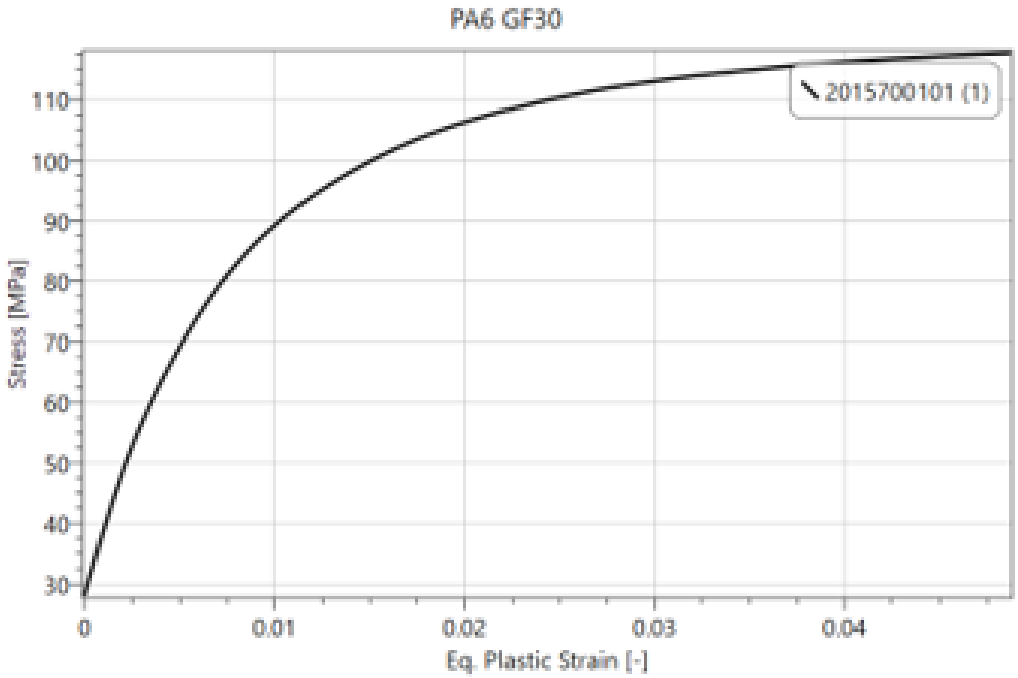

Figure B.4: Mat_157 material curve for PA6 GF30.

```
*MAT_4A_MICROMEC
$      MID     MMOPT      BUPD                              FAILM     FAILF     NUMINT
  20215001       1.0      0.01                                 0.        0.         0.
$     AOPT      MACF        XP        YP        ZP        A1        A2        A3
         0         0       0.0       0.0       0.0       0.0       0.0       0.0
$       V1        V2        V3        D1        D2        D3      BETA
       0.0       0.0       0.0       0.0       0.0       0.0        0.
$      FVF                 FL        FD                  A11       A22
      -0.3                 20       1.0                    0         0
$      ROF        EL        ET       GLT      PRTL      PRTT
2.5899e-09    70000.    70000.    28759.     0.217     0.217
$       XT                                                    SLIMXT    NCYRED
         0                                                       0.0        10
$      ROM         E        PR
  1.09e-09      1000       0.3
$    SIGYT     ETANT                            EPS0         C
         0         0                               0         0
$    LCIDT                                      LCDI       UPF
   1000001                                         0         0
```

Figure B.5: Mat_215 material card.

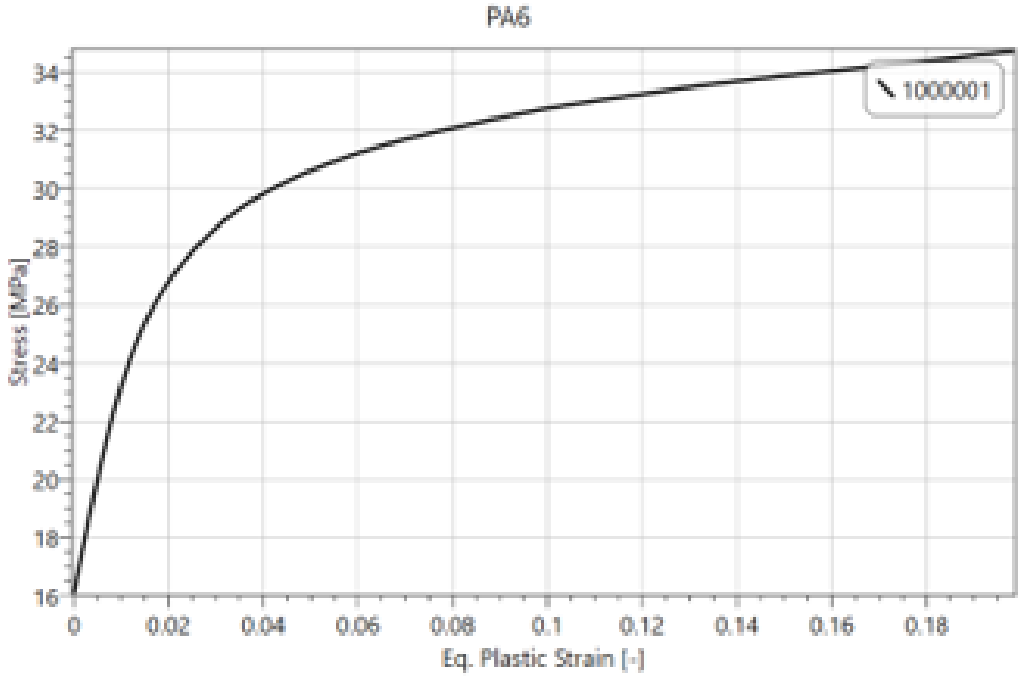

Figure B.6: Mat_215 material curve for PA6.

DEPARTMENT OF SOME SUBJECT OR TECHNOLOGY
CHALMERS UNIVERSITY OF TECHNOLOGY
Gothenburg, Sweden
www.chalmers.se

CHALMERS
UNIVERSITY OF TECHNOLOGY